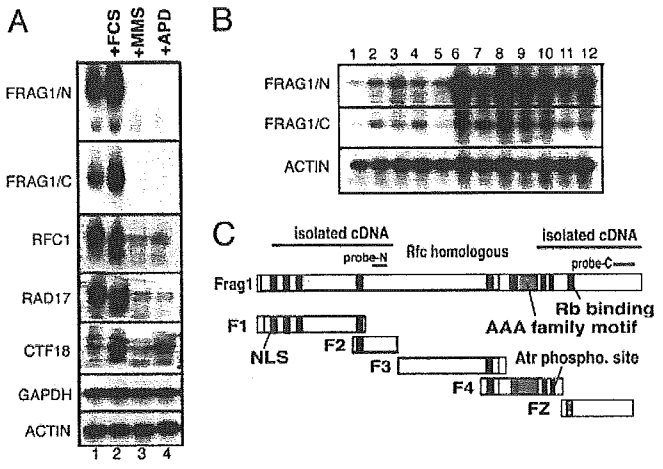

Fig. 1. Expression of the *FRAG1* gene. (*A*) RNA blot analysis. Synchronized MEFs were treated with aphidicolin, and 20 μg of each of the total RNAs were loaded on the gel, transferred to membrane, and hybridized to probes as indicated. (*B*) Frag1 expression in various mouse cell lines. Shown are poly(A)$^+$ RNA from the following sources: lane 1, PU5–1.8 (lymphoid tumor); lane 2, RAW264.7 (leukemia-virus induced tumor); lane 3, K-BALB (Kirsten murine leukemia virus-transformed fibroblast); lane 4, 3T3 (fibroblast); lane 5, L-M (murine L cells, transformed adipose connective tissue); lane 6, P19 (terato-carcinoma); lane 7, Hepa 1-6 (hepatoma); lane 8, R1.1 (T cell lymphoma); lane 9, L1210 (lymphocytic leukemia); lane 10, P388D1 (lymphoma); lane 11, P815 (mastcytoma); and lane 12, NB41A3 (neuroblastoma). (*C*) A map of Frag1 fragments. F1, F2, F3, F4, and FZ are cDNA fragments used in the study. Location of probes Frag1/N and Frag1/C in the cDNA are indicated. Rb binding motif LxCxE and two putative Atr-phosphorylation sites are located near a region homologous to the AAA family. Two locations of cDNA fragments, which were isolated through subtractive hybridization (nucleotide positions from the first methionine, 321–1835 and 3750–5388) are shown, and two probes for RNA blot analysis, which were synthesized by PCR amplification (nucleotide positions from the first methionine, 1580–1830 and 5130–5380) are shown. NLS, nuclear localization motifs.

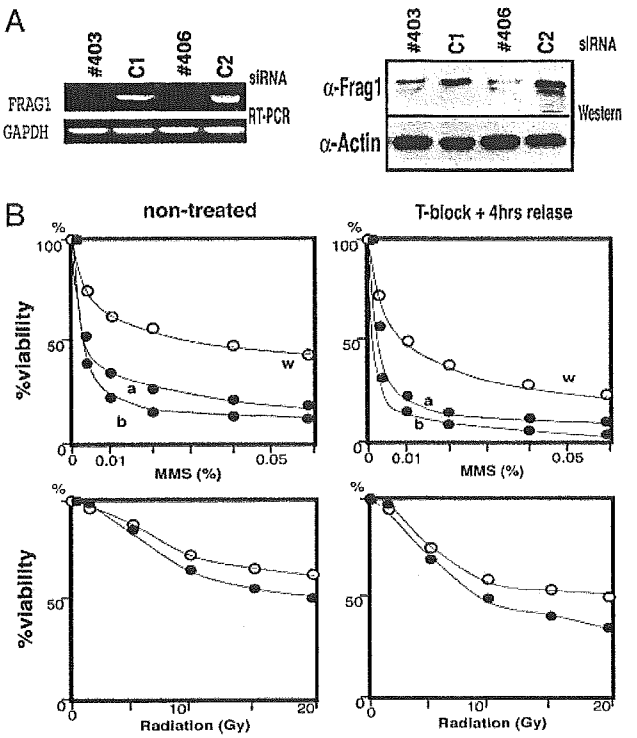

Fig. 2. Down-regulation of Frag1 expression sensitizes cells to replicative stress. (*A*) Down-regulation of *FRAG1* by siRNA. MEFs were transfected by U6 siRNA expression vector against FRAG1 and grown in selective medium. RNAs and protein lysates were extracted and analyzed by RT-PCR and immunoblot. Results of two independent experiments of *FRAG1* siRNA clones (#403 and #406) are shown. C, mock control siRNA. (*B*) Colony survival assay after exposure to MMS. Synchronized (*Right*) or asynchronized (*Left*) cells (1×10^6) were cultured in thymidine-free medium for 2 h to allow S-phase entrance. (*Upper*) MMS was added at the indicated concentrations for an additional 1 h, and cells were washed. (*Lower*) For radiation, cells were exposed at the indicated doses. Cells were plated in DMEM containing 1.5% methylcellulose, and colonies were counted 10 days after treatment. The percentage of survival was determined relative to the numbers of colonies from untreated cells. Lines labeled a and b indicate experiments with two independent siRNAs; lines labeled w indicate mock.

cells treated with actinomycin D to inhibit *de novo* RNA synthesis in medium with or without aphidicolin were harvested at serial time points and assessed for *FRAG1/N*, *FRAG1/C*, *CTF18*, *RFC*, and *RAD17* mRNA, indicating that the half-life of *FRAG1* mRNA appears to be <4 h after exposure to aphidicolin. In contrast, the half-life of *CTF18*, *RFC*, and *RAD17* mRNAs was >15 h, suggesting that *FRAG1* mRNA appeared less stable than transcripts of the other replication-related genes examined (Fig. 7 *B–E*).

Database searches indicated that the putative Frag1 protein has a conserved region homologous to a large subunit of RFC, which is considered an ortholog of the alternative RFC subunits, Elg1, Ctf18/Chl12, and Rad24 (Rad17 in fission yeast and human) of budding yeast (Fig. 1*C*) (11–14). Frag1 has a conserved AAA family motif, a hallmark of the ATPase family associated with various cellular activities, including chaperone-like functions that assist in the assembly, operation, or disassembly of protein complexes. Comparison of the mouse and human Frag1 amino acid sequences indicated that they conserve putative Atr-phosphorylation sites (mouse Frag1 at Ser-1150 and Ser-1168 and human Frag1 at Ser-1169 and Ser-1187) (18, 19), and a putative Rb binding site with a Leu-x-Cys-x-Glu (LxCxE) motif (amino acids 1409–1413 of mouse and 1428–1432 of human) (20).

Reduction of Frag1 Protein Increases Sensitivity to DNA Damage. Studies of budding yeast have shown that elg1Δ mutants are sensitive to DNA damage, suggesting that Elg1-RFC functions in the DNA damage response (11, 12). To study the effect of reduced expression of mammalian Frag1 protein, we performed siRNA experiments to inhibit expression of endogenous Frag1. RT-PCR and immunoblot study showed that cells transfected with the siRNA vector and selected in puromycin medium showed a marked reduction of Frag1 gene product (Fig. 2*A*). *FRAG1* siRNA transfectants were exposed to MMS or to γ-irradiation, and colony survival was assayed. Compared with control siRNA transfectants, two independent *FRAG1* siRNA transfectants showed enhanced sensitivity to replication stress, which was apparent in synchronized MEFs, suggesting that the damage activated the S phase checkpoint (Fig. 2*B*). The difference between siRNA knock-down and control cells after MMS treatment is more pronounced than differences observed after γ-irradiation. It is suggested that reduction of Frag1 increased the sensitivity to MMS.

Frag1 siRNA Inhibition Leads to Activation of Caspase and BAX. Immuunoblot analysis of Frag1 protein expression showed that Frag1 was reduced 2–6 h after exposure to aphidicolin or MMS, a reduction more rapid than for actin or Rad17 in MMS (Fig. 3*A*). Because involvement of Frag1 in cellular responses to DNA damage is suggested, we assessed the activation of proapoptotic proteins. Immunoblot analysis showed caspase 7 activation in *FRAG1* siRNA transfectants but not in control siRNA transfectants (Fig. 8*A*, which is published as supporting information on the PNAS web site). Bax protein expression with slow mobility was induced in two independent *FRAG1* siRNA transfectants 8 h after release from double thymidine cell cycle block and was markedly induced in

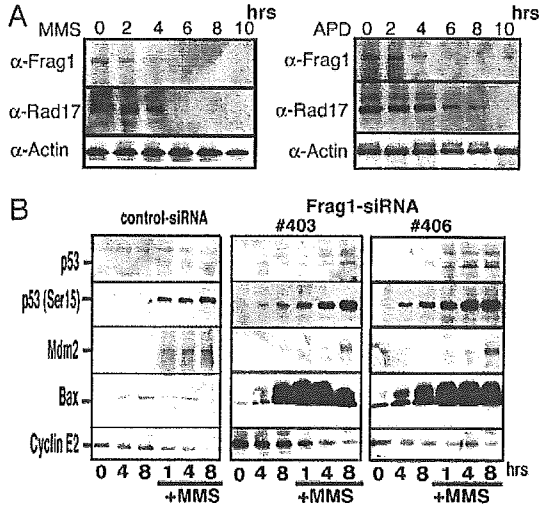

Fig. 3. Frag1 is involved in genotoxic response. (*A*) Frag1 down-regulation by genotoxic stress. MEFs were cultured in medium with 0.4 nM aphidicolin or 0.01% MMS for the indicated times. Cells were harvested, and lysates were subjected to SDS/PAGE and immunoblot analysis with antisera as indicated. (*B*) Frag1 knock-down sensitizes cells to genotoxic stress. Two independent Frag1 siRNA MEF clones (#403 and #406) synchronized in G_1 and grown in thymidine-free medium with or without exposure to MMS were harvested at the indicated times after release in thymidine-free medium. Protein lysates were immunoblotted with antibodies as indicated. Mismatched siRNA served as control.

those *FRAG1* siRNA transfectants at all times after MMS exposure. In sharp contrast, Bax induction was not apparent in control siRNA transfectants in the conditions examined (Fig. 3*B*).

Upon activation by DNA damage-induced or oncogene-induced signaling pathways, phosphorylation of p53 at Ser-15 increases its half-life, accumulation, and tumor suppressing activity (21). Phosphorylation of p53 at Ser-15 leads to reduced interaction of p53 with its negative regulator, the oncoprotein Mdm2, and impairs the ability of Mdm2 to inhibit p53-dependent transactivation (21). Our analysis of two independent Frag1 siRNA transfectants showed that phosphorylation of p53 at Ser-15 was induced in cells after MMS exposure and at 4 (Fig. 3*B*, #406) and 8 h (Fig. 3*B*, #403 and #406) without MMS. In control siRNA transfectants, phosphorylation of p53 at Ser-15 was induced in cells after, but not before, exposure to MMS, showing that, even without MMS, the reduction of Frag1 can stimulate Bax induction in synchronized cells (at 4 or 8 h), emphasizing that reduction of Frag1 sensitizes cells to genotoxic response. Alteration of Mdm2 expression was less apparent. Taken together with the observation by microscopy that cytochrome *c* was released from mitochondria when Frag1 expression was inhibited by siRNA or when cells were exposed to MMS (Fig. 8*C*), it is suggested that reduction of Frag1 may be required for sensitizing cells to DNA damage and activating Bax-related cell death.

p53 translocates to mitochondria, where it directly induces Bax activation and cytochrome *c* release upon DNA damage (22). To determine whether p53 is involved in the induction of Bax expression in our siRNA transfectants, Trp-53-deficient MEFs were analyzed. Results of siRNA Frag1 inhibition showed that Bax was induced in Trp-$53^{+/-}$ and Trp-$53^{-/-}$ transfectants of MEFs and phosphorylation of p53 at Ser-15 was increased in Trp-$53^{+/-}$ transfectants after exposure to MMS, suggesting that Bax was activated regardless of p53 status and that p53 is dispensable for Bax induction in the Frag1 replication stress pathway (Fig. 8*B*). Recently, two p53 homologues have been identified, p73 and p63, that have high amino acid identity, suggesting shared function (23).

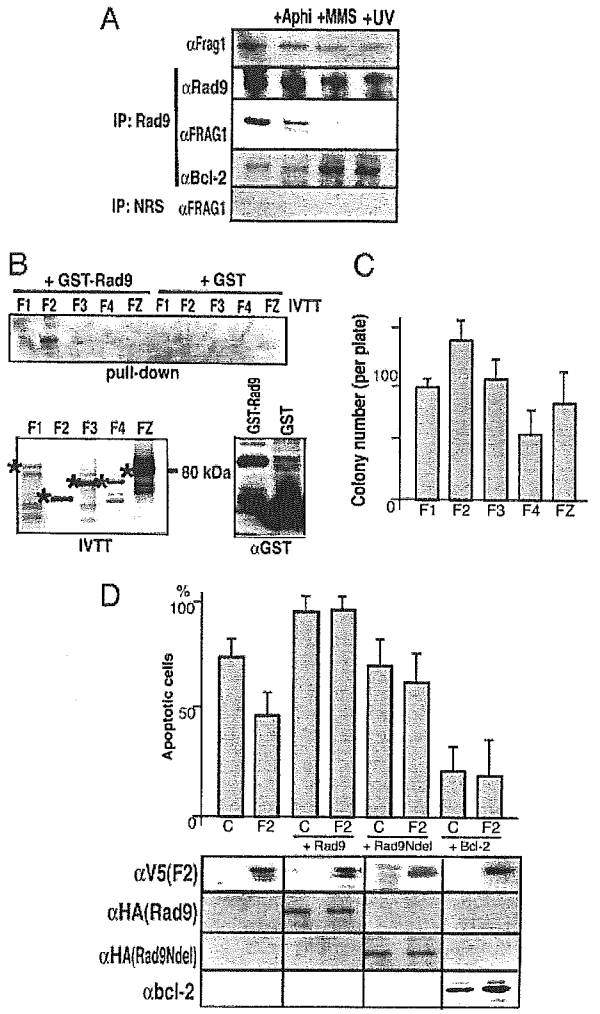

Fig. 4. Frag1 is involved in the Rad9–Bcl2 pathway. (*A*) Coimmunoprecipitation of Frag1, Rad9, and Bcl2. MEFs were grown in medium with 0.4 μM aphidicolin (Aphi) or 0.01% MMS for 24 h or exposed to 8 J/m^2 UV radiation and cultured for 24 h before harvesting. The leftmost lane is without treatment. Protein lysates were extracted and immunoprecipitated (IP) with anti-Rad9 or normal rabbit serum (NRS), followed by immunoblot with Frag1, Rad9, or Bcl2 antisera. (*B*) Pull down of *in vitro* transcribed and translated (IVTT) F1, F2, F3, F4, and FZ fragments of Frag1 by GST–Rad9 fusion protein. *In vitro* transcribed and translated products were labeled with [^{35}S]methionine and incubated with GST–Rad9 fusion protein. The bound samples were pulled down with glutathione-agarose beads, which were subjected to SDS/PAGE, and gels were exposed to x-ray film. (*Upper*) Pull-down assay. (*Lower Left*) PAGE and exposure of *in vitro* transcribed and translated F1, F2, F3, F4, and FZ fragments (input), shown by asterisks. (*Lower Right*) Immunoblot with anti-GST. (*C*) Assay of colony survival of MEF transfectants after MMS exposure. MEFs transfected with pcDNA expression vector with F1, F2, F3, F4, or FZ cDNA and selected in G418 medium were subjected to colony survival assay, similarly to that shown in Fig. 2*B*. Error bars show standard deviations. (*D*) Cell death after MMS exposure. (*Upper*) Rad9, Rad9-δN (Rad9Ndel), and Bcl2 plasmids were introduced with selection plasmids in F2 transfectants and grown in selection medium for hygromycin resistance. Apoptotic cells were evaluated 48 h after MMS exposure by erythrosine B staining exclusion. (*Lower*) Immunoblot with anti-V5 tag (F2), anti-HA tag (Rad9), anti-HA tag (Rad9Ndel), and anti-Bcl2 antisera.

Indeed, like p53, p73 can trigger several promoters, including Bax and p21 promoters, and is able to trigger cell death in response to the DNA damage. Introduction of p73 oligo siRNA into Frag1 siRNA vector transfectants of Trp-$53^{-/-}$, reduced Bax induction (data not shown), suggesting a role for p73 in the stimulation of the Frag1—Bax pathway.

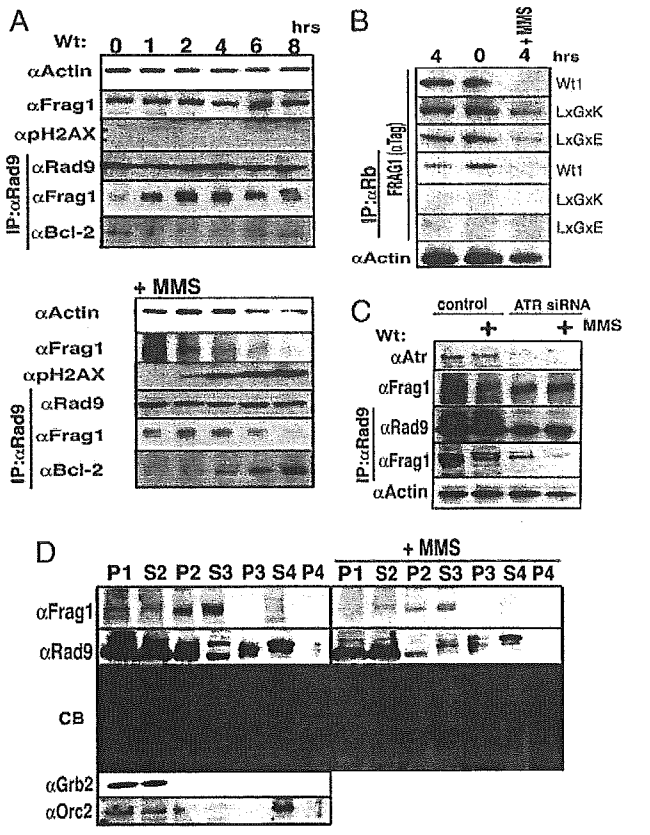

Fig. 5. Frag1 involvement in the DNA damage response. (*A*) Synchronized MEFs were cultured in growth medium with or without MMS (0.01%) for the indicated times, and cellular protein was extracted. Protein expression was studied by immunoblot with the indicated antibodies before and after immunoprecipitation (IP) with Rad9 antibody. (*B*) LxGxK, LxGxE, or wild-type (Wt) Frag1 transfectants that were synchronized at G_1 were released from G_1 in thymidine-free medium with or without MMS (0.01%) as indicated and subjected to immunoblot with anti-V5 (tag) or anti-actin antibody before and after immunoprecipitation with Rb antibody. (*C*) MEFs were transfected with Atr siRNA. A day after transfection, cells were cultured with or without MMS (0.01%) for 4 h, and protein lysates were immunoprecipitated and immunoblotted as indicated. (*D*) Subcellular localization of Frag1 and Rad9 after MMS treatment. Cellular components were fractionated from MEFs before and after exposure to MMS and subjected to immunoblot. Immunoblot with antibodies against Grb2 and Orc2, membranous and chromatin-bound proteins, are shown as controls. P1, whole-cell pellet; S2, cytosol and nucleosol; P2, detergent-insoluble nuclei; S3, DNase I-extracted nuclei; P3, DNase I-resistant fraction; S4, containing chromatin; P4, nuclear matrix. CB, Coomassie brilliant blue staining.

Frag1 Associates with Rad9 and Is Involved in the Bcl2 Pathway. It was shown that proapoptotic Bax can form heterodimers with antiapoptotic Bcl2 in cells (24), which prevents Bax conformational changes required for apoptosis induction (10). Activated Bax proteins oligomerize and are stabilized in the mitochondrial membrane and induce cytochrome *c* release, an important process for the induction of cell death (10). After DNA damage, Rad9 plays a role in induction of apoptosis by associating with antiapoptotic Bcl2, which results in the inhibition of Bcl2 function (9). To investigate the Frag1 signal pathway, we have used coimmunoprecipitation analyses (Fig. 9*A*, which is published as supporting information on the PNAS web site) to define Frag1 associations with partner proteins involved in responses to replicative stress. Immunoblots probed with anti-Frag1 after immunoprecipitation with anti-Rad9 indicated their association in growing cells. Aphidicolin or MMS exposure resulted in reduced Frag1 expression and concomitant

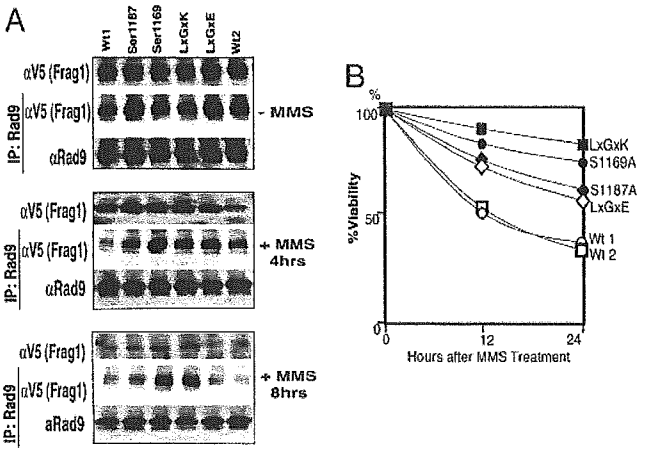

Fig. 6. The Frag1 response to DNA damage. (*A*) Association of Frag1 and Rad9 in response to DNA damage. Wild-type (Wt) and Frag1 mutant MEF transfectants synchronized at G_1 were released from G_1 in thymidine-free medium with 0.01% MMS for 4 or 8 h. Cellular lysates were extracted and subjected to immunoblot with anti-V5 (tag) or anti-actin antibody before and after immunoprecipitation (IP) with Rb antibody. (*B*) Viability of cells expressing wild-type and Frag1 mutants after MMS exposure. Wild-type and Frag1 mutant-expressing MEFs were cultured in medium with 0.01% MMS for the indicated times, and apoptotic cells were evaluated by erythrosine B staining exclusion.

reduction of the association with Rad9. Conversely, an increase of Rad9 association with Bcl2 was observed after genotoxic stress (Fig. 4*A*). *In vitro* pull-down assay using recombinant GST–Rad9 fusion protein detected association with *in vitro* transcribed–translated Frag1-F2 fragment, corresponding to the RFC homologous region. Other Frag1 fragments did not associate with Rad9 (Figs. 1*C* and 4*B*), suggesting that the F2 fragment binds Rad9 and regulates apoptosis induction.

Colony formation assays of MEF transfectants expressing specific Frag1 peptides indicated that more colonies formed after F2 expression compared with other Frag1 peptides after genotoxic stress (Fig. 4*C*), suggesting that the F2 region of Frag1 functions to regulate apoptosis by interacting with Rad9. The stable F2 transfectants, in which MMS-induced apoptosis was inhibited, were transfected with Rad9 and selected for hygromycin resistance (Fig. 4*D Upper*, compare F2 and C). Overexpression of Rad9 in the F2 expressors caused an increase in apoptosis (Fig. 4*D*, +RAD9). Usage of Rad9-δN, which is defective in Bcl2 association (9), inhibited apoptosis (Fig. 4*D*, +Rad9Ndel). Furthermore, introduction of antiapoptotic Bcl2 into F2 transfectants resulted in profound inhibition of apoptosis (+Bcl2). Confocal microscopy showed that in F2 transfectants release of cytochrome *c* after exposure to MMS was inhibited (Fig. 9*B*). Results of these experiments strongly suggest that Frag1 modulates Rad9 association with Bcl2 and thereby induces DNA damage-induced apoptosis.

Atr Regulates Frag1–Rad9 Association and the Release of Rad9 from Frag1 in S Phase. To further define Frag1 function, we examined the cell cycle-dependence of Frag1 association with Rad9 in synchronized cells exposed to MMS. Association of Frag1 with Rad9 was weak in synchronized G_1 cells and increased in strength during progression into S phase. After exposure to MMS, the Frag1–Rad9 association was reduced, leading to an increase of Rad9–Bcl2 association (Fig. 5*A*). The data are consistent with the conclusion that Frag1 is involved in sensitizing Rad9 to genotoxic stress during S phase through their association. Confocal microscopic observation indicated that Frag1 and Atr are colocalized 8–12 h after exposure to MMS, whereas Frag1 seems to form foci before Atr focus formation (Fig. 10, which is published as supporting infor-

mation on the PNAS web site), suggesting a role for Frag1 in the Rad9 pathway via Atr response to DNA damage.

To study further the involvement suggested by the Frag1 motif search (Fig. 1*C*) of Atr and Rb in the Frag1–Rad9 pathway, we prepared wild-type and mutant human Frag1 expression vectors by substituting the putative Atr phosphorylation sites, Ser-1169 and Ser-1187 with Ala residues, and the Rb-binding site, LxCxE-1432 with LxGxK-1432 or LxGxE-1432. Transfected wild-type Frag1, but not LxGxE and LxGxK mutants, associated with Rb, as was more apparent in synchronized G_1 than S phase cells (Fig. 5*B*). After MMS, wild-type Frag1 expression was undetectable, whereas LxGxK, and to a lesser extent LxGxE, mutant proteins were detectable. The Frag1–Rb association was undetectable in wild type and two Rb-site mutants after MMS. In summary, it is suggested that Frag1 might play a role in pre-sensitizing cells to genotoxic stress during replication, i.e., in S phase, whereas Frag1 predominantly associates with Rb in G_1 phase.

To examine the role of Atr, endogenous Atr was inhibited by siRNA (Fig. 5*C*). Whereas MMS damage reduced endogenous Frag1 in control cells, reduction of Atr inhibited the down-regulation of endogenous Frag1 in response to DNA damage. Immunoprecipitation showed that, in response to MMS exposure, inhibition of Atr markedly reduced the association of Rad9 with Frag1, a reduction in siRNA ATR-treated cells that was more appreciable than in control cells. Thus, Atr stimulated two separable events: association of Rad9 with Frag1 and down-regulation of Frag1 in response to DNA damage.

Cellular components before and after MMS exposure were fractionated, and proteins were analyzed by immunoblot to study the translocation of Rad9 in response to DNA damage (Fig. 5*D*). After exposure to MMS, the amount of Rad9 in detergent-insoluble nuclei (P2) was significantly reduced, and the proportion of slow mobility Rad9 was increased in DNase I-extracted nuclei (S3), whereas reduction but not translocation of Frag1 was detected, suggesting that a predominant fraction of Rad9 translocated from chromatin to soluble fraction. These results suggest that Frag1 has a role in loading activated Rad9 onto damaged chromatin and stimulating its translocation.

To determine whether phosphorylation and Rb-binding of Frag1 are involved in the association and release of Rad9 (Fig. 6*A*), stable transfectants expressing Frag1 or Frag1 mutants were exposed to MMS, and protein lysates were analyzed by immunoblot. Association of Frag1 with Rad9 was reduced 4 and 8 h after cells were released from G_1 block and exposed to MMS; however, the reduction was inhibited in the Ser-1169A and LxGxK mutants and, to a lesser extent, in Ser-1187A and LxGxE mutants, suggesting that Atr phosphorylation stimulates the dissociation of Rad9 and that Rb binding is also involved, directly or indirectly, in Rad9 activation. The evaluation of apoptotic cells showed that the mutants, especially Ser-1169A and LxGxK, had DNA damage-resistant phenotypes compared with wild-type transfectants (Fig. 6*B*), emphasizing the importance of the Frag1–Rad9 association to apoptosis induction. We finally assessed cotransfectants with Frag1 and wild-type or kinase-dead ATR. Immunoblot analysis showed that, after MMS exposure, down-regulation of Frag1 was inhibited by kinase-dead ATR but not by wild-type ATR (data not shown), supporting the conclusion that phosphorylation by Atr plays a role in the Frag1–Rad9-regulated DNA damage response.

As for a mechanism, our data showed that Frag1 amino acids Ser-1169 and Ser-1187 play critical roles in the regulation of Rad9 release and cell death in response to DNA damage. Ser-1169 and Ser-1187 are putative phosphorylation sites for Atr, which is a sensor of stalled or collapsed replication forks at mid-S phase checkpoint (19). Overexpression of a Rad9-associated Frag1 polypeptide inhibited Bcl2 family-mediated apoptosis, suggesting that Frag1 functions as a platform for loading Rad9 to damaged lesions. As shown in the present study of *ATR* siRNA, after genotoxin exposure, reduction of Atr inhibited the down-regulation of endogenous Frag1 and markedly reduced association of Rad9 with Frag1, suggesting that the loading of Rad9 onto damaged chromatin by Frag1 may require Atr and that Atr could down-regulate Frag1 through phosphorylation sites Ser-1169 and Ser-1187. As for the activation of Rad9, earlier studies showed several mechanisms for recruiting Rad9 to damaged lesions, including Abl-mediated phosphorylation of Rad9, which induced binding of Rad9 to antiapototic BclxL (25); PKCδ phosphorylation of Rad9 after genotoxin exposure (26); and MEC1 and TEL1 of budding yeast, homologues of Atr and Atm, which regulate Rad9 hyperphosphorylation (27). Thus, Atr, in concert with those molecules, can play a direct or indirect role in recruiting Rad9 onto Frag1. Full execution of the steps could lead to the stimulation of the Rad9–Bcl2 cell death pathway. We propose a schema in which each step participates in sensing damage, activating checkpoint, and execution of apoptosis; the multisteps may compose the machinery for the pathway, which determines the fate of cells with perturbations in DNA replication progression, i.e., whether the DNA damage is compatible with cell survival or requires elimination by apoptosis (Fig. 11, which is published as supporting information on the PNAS web site).

We thank Drs. Stuart Schreiber and Karlene Cimprich for kindly providing the plasmids pBJF-ATRwt and pBJF-ATRkd, Drs. Yutaka Eguchi and Yoshihide Tsujimoto for kindly providing pCAGGS-hbcl-2, and Dr. Hong Gang Wang for HA-Rad9 and Flag-Rad9-δN. This work was supported in part by research funds from the High-Tech Research Center Project of the Ministry of Education, Culture, Sports, Science and Technology of Japan, the Mochida Memorial Foundation, and the Cell Science Research Foundation.

1. Rothstein, R., Michel, B. & Gangloff, S. (2000) *Genes Dev.* **14**, 1–10.
2. Bakkenist, C. J. & Kastan, M. B. (2004) *Cell* **118**, 9–17.
3. Levitt, N. C. & Hickson, I. D. (2002) *Trends Mol. Med.* **8**, 179–186.
4. Parrilla-Castellar, E. R., Arlander, S. J. & Karnitz, L. (2004) *DNA Repair* **3**, 1009–1014.
5. Kaina, B. (2003) *Biochem. Pharmacol.* **66**, 1547–1554.
6. Dang, T., Bao, S. & Wang, X. F. (2005) *Genes Cells* **10**, 287–295.
7. Hang, H. & Lieberman, H. B. (2000) *Genomics* **65**, 24–33.
8. Zou, L., Cortez, D. & Elledge, S. J. (2002) *Genes Dev.* **16**, 198–208.
9. Komatsu, K., Miyashita, T., Hang, H., Hopkins, K. M., Zheng, W., Cuddeback, S., Yamada, M., Lieberman, H. B. & Wang, H. G. (2000) *Nat. Cell Biol.* **2**, 1–6.
10. Kirkin, V., Joos, S. & Zornig, M. (2004) *Biochim. Biophys. Acta* **1644**, 229–249.
11. Bellaoui, M., Chang, M., Ou, J., Xu, H., Boone, C. & Brown, G. W. (2003) *EMBO J.* **22**, 4304–4313.
12. Ben-Aroya, S., Koren, A., Liefshitz, B., Steinlauf, R. & Kupiec, M. (2003) *Proc. Natl. Acad. Sci. USA* **100**, 9906–9911.
13. Kanellis, P., Agyei, R. & Durocher, D. (2003) *Curr. Biol.* **13**, 1583–1595.
14. Smolikov, S., Mazor, Y. & Krauskopf, A. (2004) *Proc. Natl. Acad. Sci. USA* **101**, 1656–1661.
15. Merrick, C. J., Jackson, D. & Diffley, J. F. (2004) *J. Biol. Chem.* **279**, 20067–20075.
16. Montes de Oca, R., Andreassen, P. R., Margossian, S. P., Gregory, R. C., Taniguchi, T., Wang, X., Houghtaling, S., Grompe, M. & D'Andrea, A. D. (2005) *Blood* **105**, 1003–1009.
17. Bell, S. P. & Dutta, A. (2002) *Annu. Rev. Biochem.* **71**, 333–374.
18. O'Neill, T., Dwyer, A. J., Ziv, Y., Chan, D. W., Lees-Miller, S. P., Abraham, R. H., Lai, J. H., Hill, D., Shiloh, Y., Cantley, L. C., *et al.* (2000) *J. Biol. Chem.* **275**, 22719–22727.
19. Abraham, R. T. (2001) *Genes Dev.* **15**, 2177–2196.
20. Pennaneach, V., Salles-Passador, I., Munshi, A., Brickner, H., Regazzoni, K., Dick, F., Dyson, N., Chen, T. T., Wang, J. Y., Fotedar, R., *et al.* (2001) *Mol. Cell.* **7**, 715–727.
21. Shieh, S. Y., Ikeda, M., Taya, Y. & Prives, C. (1997) *Cell* **91**, 325–334.
22. Chipuk, J. E., Kuwana, T., Bouchier-Hayes, L., Droin, N. M., Newmeyer, D. D., Schuler, M. & Green, D. R. (2004) *Science* **303**, 1010–1014.
23. De Laurenzi, V. & Melino, G. (2000) *Ann. N.Y. Acad. Sci.* **926**, 90–100.
24. Oltvai, Z. N., Milliman, C. L. & Korsmeyer, S. J. (1993) *Cell* **74**, 609–619.
25. Yoshida, K., Komatsu, K., Wang, H. G. & Kufe, D. (2002) *Mol. Cell. Biol.* **22**, 3292–3300.
26. Yoshida, K., Wang, H. G., Miki, Y. & Kufe, D. (2003) *EMBO J.* **22**, 1431–1441.
27. Vialard, J. E., Gilbert, C. S., Green, C. M. & Lowndes, N. F. (1998) *EMBO J.* **17**, 5679–5688.

Available online at www.sciencedirect.com
SCIENCE DIRECT®
Biochemical Pharmacology 69 (2005) 1585–1594
Biochemical Pharmacology
www.elsevier.com/locate/biochempharm

Relative importance of apoptosis and cell cycle blockage in the synergistic effect of combined R115777 and imatinib treatment in BCR/ABL-positive cell lines

Takuji Miyoshi [a], Tadashi Nagai [a,*], Ken Ohmine [a], Makiko Nakamura [a], Yasuhiko Kano [b], Kazuo Muroi [c], Norio Komatsu [a], Keiya Ozawa [a]

[a] *Division of Hematology, Jichi Medical School, 3311-1 Yakushiji, Minamikawachi-machi, Kawachi-gun, Tochigi 329-0498, Japan*
[b] *Division of Hematology and Medical Oncology, Tochigi Cancer Center, Tochigi, Japan*
[c] *Cell Transplantation and Transfusion, Jichi Medical School, Tochigi, Japan*

Received 13 September 2004; accepted 9 February 2005

Abstract

The combination of imatinib and a farnesyltransferase inhibitor might be effective for reducing the number of BCR/ABL-positive leukemia cells. In this study, we examined the differences in the mechanisms of the growth inhibitory effect of the combination of imatinib and R115777 (Zarnestra™) among BCR/ABL-positive cell lines. Steel and Peckham isobologram analysis indicated that this combination had a strong synergistic inhibitory effect on growth in all imatinib-resistant cell lines and their parental cell lines. Levels of cleaved caspase 3 were increased by the combination treatment in all cell lines. However, both the level of cleaved PARP and the number of annexin-V-positive cells were much less increased in KCL22 and KCL22/SR cells than in K562, KU812, K562/SR and KU812/SR cells. The combination treatment promoted $p27^{KIP1}$ accumulation and induced a significant increase in the percentage of G0/G1 KCL22 and KCL22/SR cells. In other cell lines, the percentage of G0/G1 cells was not increased but rather decreased. The results indicate that induction of apoptosis and blockage of the cell cycle were major mechanisms of the synergistic inhibitory effect of the combination treatment, but the relative importance of these mechanisms differed among cell types. Additional treatment for overriding the G1 checkpoint may be required to eradicate leukemia cells, in which the combination induces cell cycle arrest.

Keywords: R115777; Farnesyltransferase inhibitor; Imatinib; BCR/ABL; Chronic myeloid leukemia; Drug resistance

1. Introduction

The ABL tyrosine kinase inhibitor imatinib mesylate (imatinib, Novartis) has shown a substantial clinical effect in BCR/ABL-positive leukemia patients [1–4]. It has been reported that about 50% of patients with aggressive BCR/ABL-positive leukemia, such as chronic myeloid leukemia in blast crisis (CML-BC) and acute lymphoblastic leukemia (ALL), exhibit a hematological response to treatment with imatinib alone [3,4]. However, most patients with such leukemia relapse soon after showing a response to imatinib; thus, long-term remission is not obtained with imatinib treatment alone. Furthermore, it is possible that many patients with CML-BC will have primary resistance to imatinib because imatinib may already have been administered in the chronic phase in many cases. Previous studies have demonstrated that BCR/ABL gene amplification, point mutations in the ATP-binding pocket of the BCR/ABL gene, increased expression of BCR/ABL protein, up-regulation of P-glycoprotein (P-gp) belonging to the ABC transporter family, increased concentration of serum α1 acid glycoprotein and up-regulation of Nrf2-mediated gene expressions may be involved in the acquisition of resistance to imatinib [5–14]. Several recent studies have indicated that imatinib-resistant cells with a point mutation in the BCR/ABL gene may be present prior to treatment with imatinib in BCR/ABL-positive leukemia patients [5,15–17]. Therefore, to obtain a sufficient clinical effect, it is important to reduce the number of imatinib-resistant leukemia cells by initial treatment targeting aggressive BCR/ABL-positive leukemia. Recently, a new generation of BCR/ABL kinase inhibitors has been developed [18–21] and has been shown to be effective

* Corresponding author. Tel.: +81 285 58 7353; fax: +81 285 44 5258.
E-mail address: t-nagai@jichi.ac.jp (T. Nagai).

0006-2952/$ – see front matter © 2005 Elsevier Inc. All rights reserved.
doi:10.1016/j.bcp.2005.02.021

against imatinib-resistant cells with point mutations in vitro [18]. However, none of these inhibitors are currently available for clinical use. At present, one attractive therapeutic strategy is combination therapy with imatinib and other anti-leukemia reagents. Cytotoxic effects of various combinations on leukemia cells have been investigated [22,23].

Some cellular proteins, including Ras family proteins, require posttranslational modifications to become active. Prenylation, which is involved in these modifications, can be performed by adding a 15-carbon farnesyl isoprenoid group mediated by farnesyltransferase. An alternative prenylation reaction, geranylgeranylation, can be performed by transferring a 20-carbon geranylgeranyl isoprenoid to proteins by geranylgeranyl transferases. Because prenylation is required to transfer Ras proteins to the cellular membrane, farnesyltransferase inhibitors (FTIs) were initially expected to suppress Ras function, leading to tumor growth inhibition [24,25]. An FTI showed significant anti-tumor activity via inhibition of H-Ras function in an activated H-Ras-induced breast cancer model [26]. However, N-Ras and K-Ras can be transferred to the cellular membrane by geranylgeranylation, even if farnesylation is inhibited, suggesting that inhibition of the processing of other target proteins is involved in the anti-tumor effects of FTIs. Such target proteins may include the small GTP-binding protein RhoB and the centromere-associated proteins CENP-E and CENP-F [27,28].

FTIs have been shown to have anti-leukemia effects on BCR/ABL-positive cultured cells and in BCR/ABL-positive murine models [29,30]. Moreover, Hoover et al. reported that an FTI, SCH66336, inhibited proliferation of imatinib-resistant cell lines and colony formation by hematopoietic progenitors from imatinib-resistant CML patients [31]. These findings suggest that FTIs have potential as agents for treatment of imatinib-resistant BCR/ABL-positive leukemia. The results of clinical studies on an FTI, R115777 (Zarnestra™, Titusville, NJ), indicate that it is moderately effective against CML [32,33]. However, R115777 alone does not seem to be sufficiently effective against aggressive CML [33]. Phase I studies using combination therapy with R115777 and imatinib for treatment of refractory or resistant BCR/ABL-positive leukemia have been conducted [34,35].

In this study, we investigated the mechanisms underlying the inhibitory effect of the combination of R115777 and imatinib on growth of BCR/ABL-positive cells. Our isobologram analysis revealed that this combination has a significant synergistic inhibitory effect on growth of imatinib-resistant cell lines and imatinib-sensitive cell lines. We also found that this effect was due to both induction of apoptosis and blockage of the cell cycle, but the relative importance of these two mechanisms differed among cell lines.

2. Materials and methods

2.1. Cell lines

We previously established an imatinib-resistant clone, KCL22/SR, from the KCL22 human BCR/ABL-positive cell line [36]. To obtain other imatinib-resistant clones, we treated K562 and KU812 cells (BCR/ABL-positive cell lines established from peripheral blood of CML patients in blast crisis) with step-wise increasing concentrations of imatinib (0.1–1.0 μM) and cultured them on a medium containing methylcellulose, followed by selection and cloning of individual colonies. These newly cloned imatinib-resistant cell lines were designated K562/SR and KU812/SR, respectively. All imatinib-sensitive parental cells and imatinib-resistant cells were grown in RPMI1640 medium supplemented with 10% fetal bovine serum and split every 4 days.

2.2. Cytotoxic effects of a combination of R115777 and imatinib

The farnesyltransferase inhibitor R115777 was kindly provided by Johnson & Johnson Pharmaceutical and Development (Philadelphia, PA). Imatinib was purchased from Novartis Pharma (Basel, Switzerland). Cells were incubated with various concentrations of each reagent for 4 days and then cell numbers were counted using a Cell Counting Kit-8 (Wako Pure Chemical Industries Ltd. Osaka, Japan) in accordance with the manufacturer's instructions. The cytotoxic effect of the combination of R115777 and imatinib was evaluated by a Steel and Peckham isobologram as described previously [37,38]. When the points were outside the left margin of the envelope formed by two broken lines, the combination treatment was considered to have a synergistic effect on cell growth inhibition. If the points were plotted within the envelope, the combination treatment was considered to have an additive effect.

2.3. Western blot analysis

Whole cell lysates were prepared from 1×10^7 cells according to a method described previously [39]. Then 10 μg of whole cell lysate was separated electrophoretically using 10% polyacrylamide gel. Immunoblotting and detection by enhanced chemiluminescence were performed as described previously [40]. Mouse anti-glyceraldehyde-3-phosphate dehydrogenase monoclonal antibody and anti-phospho-tyrosine antibody were purchased from Chemicon International (Temecula, CA) and Santa Cruz Biotechnology (Santa Cruz, CA), respectively. Anti-cleaved caspase 3, anti-PARP, anti-p44/42 (ERK1/2) MAP kinase and anti-phospho p44/42 (ERK1/2) MAP kinase rabbit polyclonal antibodies were purchased from Cell Signaling Technology (Beverly, MA). Mouse anti-

$p27^{KIP1}$ and anti-HDJ-2 monoclonal antibodies were purchased from BD Biosciences (San Jose, CA) and Neomarkers (Fremont, CA), respectively.

2.4. Flow cytometry

Apoptotic cells were evaluated by counting annexin-V-positive cells using a MEBCYTO-Apoptosis Kit (MBL, Nagoya, Japan) in accordance with the manufacturer's instructions. Briefly, the cells were collected and rinsed once with phosphate-buffered saline (PBS). The cells were then incubated with annexin-V-FITC and propidium iodide for 15 min and analyzed by flow cytometry using a FACScan Analyzer (Becton Dickinson, San Jose, CA). For cell cycle analysis, the cells were incubated with propidium iodide for 30 min and analyzed by flow cytometry using a FACScan/CellFIT system (Becton Dickinson, San Jose, CA).

3. Results

3.1. Development of imatinib-resistant BCR/ABL-positive cell lines

We used an imatinib-resistant clone, KCL22/SR, and its parental BCR/ABL-positive cell line, KCL22 [36]. In addition, we cloned two other imatinib-resistant clones, K562/SR and KU812/SR, from the BCR/ABL-positive cell lines K562 and KU812, respectively. As shown in Table 1, IC_{50} values of imatinib against the three imatinib-resistant clones were 5–9-fold higher than that against each corresponding parental cell line. No amplification of or point mutation in the BCR/ABL gene was found in these imatinib-resistant clones. Consistent with our previous findings [36], imatinib treatment resulted in a significant decrease in the level of phosphorylation of BCR/ABL protein in all imatinib-resistant clones as well as parental cell lines (data not shown). These results suggest that deregulation of processes downstream of BCR/ABL kinase is involved in the acquisition of resistance to imatinib in these imatinib-resistant clones.

3.2. Combined treatment of BCR/ABL-positive cells with R115777 and imatinib resulted in synergistic inhibition of cell growth

To confirm that the farnesyltransferase inhibitor R115777 inhibits farnesylation in BCR/ABL-positive cells, we examined the level of the chaperone protein HDJ-2, which is a substrate of farnesyltransferase, by Western blot analysis using an anti-HDJ-2 antibody [41]. Treatment of cells with R115777 resulted in significant accumulation of unprocessed HDJ-2 in all cell lines (data not shown), suggesting that farnesylation is effectively inhibited by R115777 in both imatinib-sensitive and imatinib-resistant BCR/ABL-positive cells. To determine whether a combination of R115777 and imatinib effectively inhibits growth of BCR/ABL-positive cells, we examined the time courses of changes in cell count after treatment with IC_{50} concentrations of imatinib, R115777 and a combination of these two reagents. The combined treatment resulted in greater suppression of cell growth than did treatment with either of the reagents alone in all parental and imatinib-resistant cells (data not shown). To determine whether the growth inhibitory effect was synergistic or additive, we next performed Steel and Peckham isobologram analysis, which provides very strict and reliable results [38]. Combined treatment of parental cells (KCL22, K562 and KU812) with R115777 and imatinib resulted in clear synergistic inhibition of cell growth (Fig. 1A). This combination also synergistically inhibited the growth of imatinib-resistant cells, KCL22/SR, K562/SR and KU812/SR (Fig. 1A). These results indicate that the combination of R115777 and imatinib has a synergistic inhibitory effect on growth of BCR/ABL-positive cells, regardless of sensitivity to imatinib.

R115777 was initially expected to be an inhibitor of Ras function. We investigated the levels of phosphorylation of ERK1/2, a Ras-mitogen-activated protein kinase (MAPK), to determine whether the synergistic inhibitory effect was mediated by alteration of Ras signaling. However, the levels of phopho-ERK1/2 were not decreased by R115777 treatment in any of the cell lines (data not shown). These results suggest that inhibition of Ras-MAPK signaling is not involved in the inhibitory effect of R115777 on BCR/ABL-positive cells.

Table 1
IC_{50} values of imatinib against the imatinib-sensitive and the imatinib-resistant cell lines

IC_{50} values(μM)		
KCL22 0.199 ± 0.037	KCL22/SR 1.779 ± 0.934	Ratio ×8.940
K562 0.218 ± 0.091	K562/SR 1.245 ± 0.419	Ratio ×5.711
KU812 0.216 ± 0.076	KU812/SR 1.526 ± 0.308	Ratio ×7.065

3.3. R115777 and imatinib synergistically inhibited the growth of leukemia cells from a patient in blast crisis

We next examined the effect of combined treatment on the growth of primary leukemia cells from a 53-year-old male patient in imatinib-resistant blast crisis. Written informed consent for the examination was obtained from the patient. Leukemia cells from peripheral blood of the patient, with no mutation in the BCR/ABL gene, were used for Steel and Peckham isobologram analysis. The patient showed no response to imatinib after conversion to blast crisis. The IC_{50} of imatinib to these cells was 0.71 μM, which is high compared with those of imatinib-sensitive CML cell lines. Combined treatment of these cells with R115777 and imatinib resulted in a synergistic inhibitory effect on growth (Fig. 1B). These results suggest that this combination treatment is effective against primary imati-

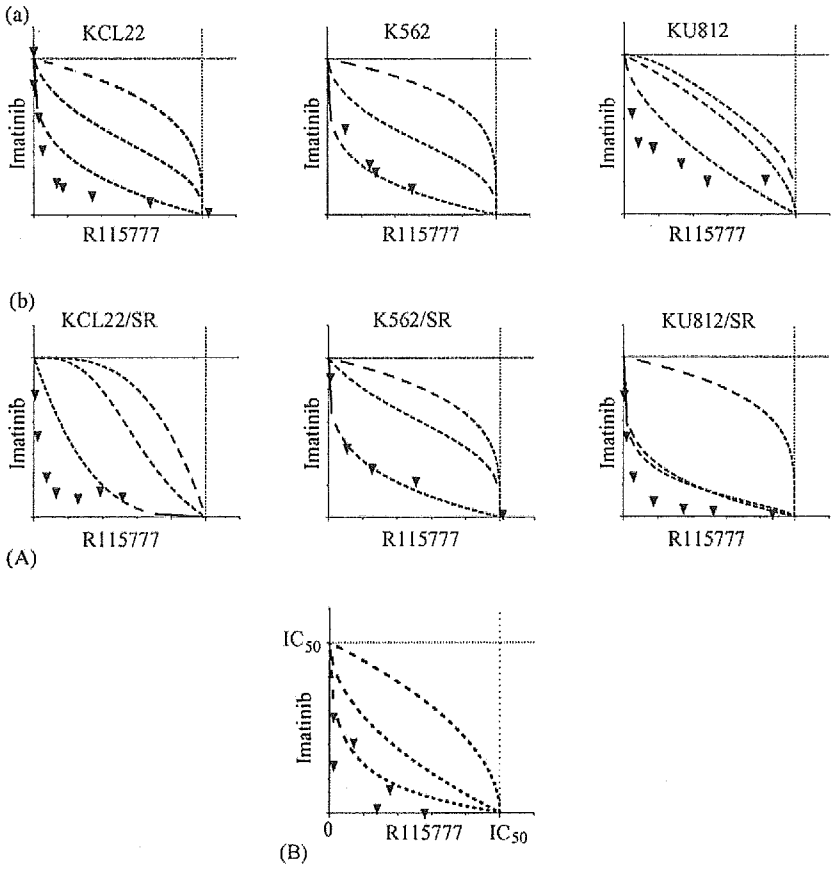

Fig. 1. Effect of combination of R115777 and imatinib on growth inhibition. (A) Steel and Peckham isobologram analyses of the combination of R115777 and imatinib in BCR/ABL-positive cell lines were performed as described in Section 2. Most points are plotted in the area representing synergistic effects in all BCR/ABL-positive parental cell lines (a) and imatinib-resistant cell lines (b). (B) Mononuclear cells from peripheral blood of a patient with imatinib-refractory blast crisis were first seeded at a density of 1×10^5 cells/ml and cultured in RPMI1640 media for 72 h. Steel and Peckham isobologram analysis of the combination of R115777 and imatinib was performed as described in Section 2. Most points are plotted in the area of synergistic effects.

nib-resistant BCR/ABL-positive cells in patients in blast crisis.

3.4. Induction of apoptosis by combination of R115777 and imatinib

To clarify whether the combination of R115777 and imatinib inhibits cell growth due to induction of apoptosis, we examined the levels of cleaved caspase 3, cleaved PARP and the number of annexin-V-positive cells with or without the combination treatment. The combination treatment increased the level of cleaved caspase 3 in all parental and imatinib-resistant cell lines (Fig. 2A). In K562, K562/SR, KU812 and KU812/SR cells, the level of cleaved PARP, which is one of the downstream molecules of caspase 3, was also significantly increased. Consistent with these results, the combination treatment markedly increased the number of annexin-V-positive K562, K562/SR, KU812 and KU812/SR cells, whereas addition of IC_{50} concentrations of imatinib or R115777 alone only slightly increased the number of annexin-V-positive cells (Fig. 2B). In contrast, the level of cleaved PARP was much less increased by the combination treatment in KCL22 and KCL22/SR cells (Fig. 2A). Furthermore, induction of annexin-V-positive cells was much less pronounced in KCL22 and KCL22/SR cells at 72 h (Fig. 2B), 48 h and 96 h (data not shown) after addition of R11577 with imatinib. These results indicate that the combination of R11577 and imatinib induces apoptosis in both imatinib-sensitive and imatinib-resistant cells, but the contribution of apoptosis to the synergistic inhibitory effect on cell growth is relatively low in KCL22 and KCL22/SR cells because of insufficient activation of PARP.

3.5. Effect of the combination of R115777 and imatinib on the cell cycle

Since the combination treatment only slightly increased the number of annexin-V-positive cells in KCL22 and KCL22/SR cells, we hypothesized that the synergistic growth inhibition was mainly caused by induction of cell cycle blockage in these cells. To investigate the function of the G1 checkpoint, we first examined the level of $p27^{KIP1}$. Consistent with our previous findings, $p27^{KIP1}$ expression was up-regulated by treatment with imatinib alone in

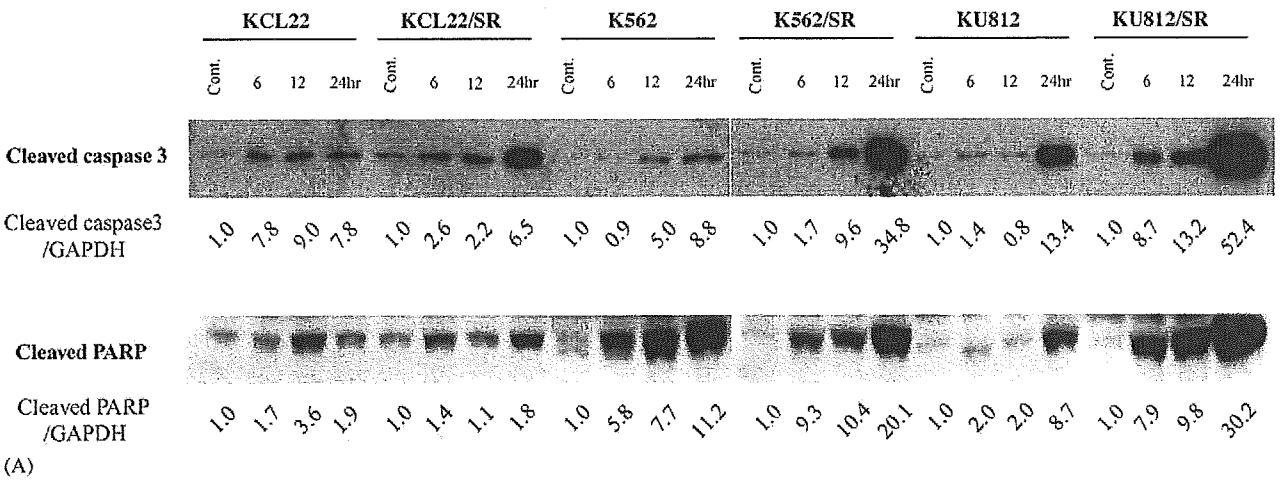

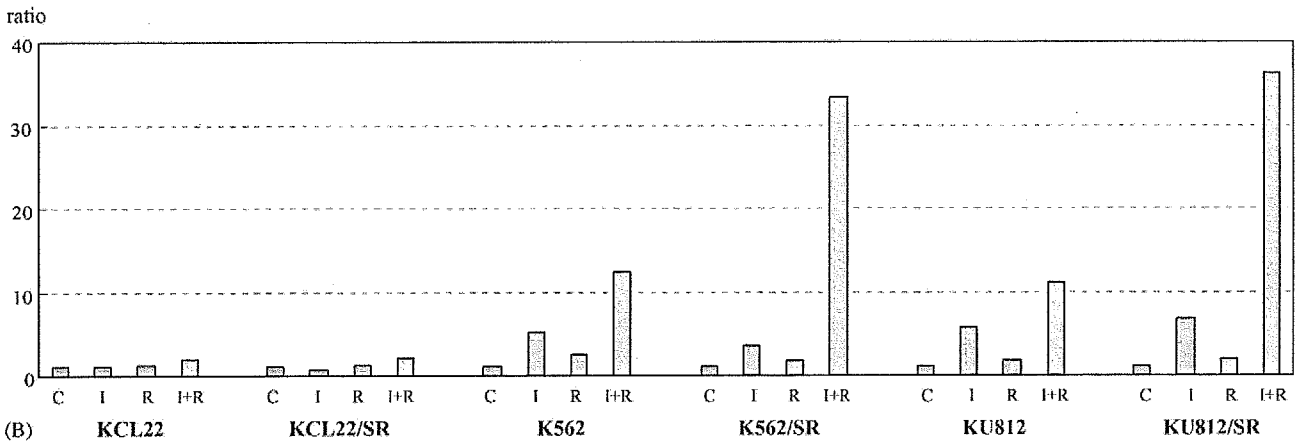

Fig. 2. Induction of apoptosis by a combination of R115777 and imatinib. (A) Cells were cultured in the absence of any reagent for 3 days prior to the treatment and then treated with a combination of IC_{50} concentrations of imatinib and R115777 for 6, 12 and 24 h. Total cell lysates were prepared and subjected to Western blot analysis using anti-cleaved casepase-3 and anti-PARP antibodies. The expression of glyceraldehyde-3-phosphate dehydrogenase (GAPDH) was examined as an internal control. The levels of cleaved caspase 3 and cleaved PARP normalized on the basis of GAPDH levels are shown. (B) Cells were cultured in the absence of any reagent for 3 days prior to treatment and then treated with IC_{50} concentrations of imatinib, R115777 or a combination of imatinib and R115777 for 72 h. The number of annexin-V-positive cells was counted by flow cytometry as described in Section 2.

KCL22 and KCL22/SR cells (Fig. 3A). In these cells, the combination treatment with IC_{50} concentrations of R115777 and imatinib also promoted $p27^{KIP1}$ accumulation and significantly increased the percentage of G0/G1 cells (Fig. 3A and B). To determine whether a higher concentration of imatinib could induce cell cycle progression and thus lead cells to apoptosis, we next examined the effect of combined treatment with 5 μM imatinib and IC_{50} concentration of R115777 on $p27^{KIP1}$ expression and G0/G1 accumulation. The results showed that the combination of the reagents at these concentrations increased $p27^{KIP1}$ level and the percentage of G0/G1 cells to the same level and percentage as those in the case of IC_{50} concentrations of R115777 and imatinib (data not shown). These findings suggest that the combination could not abrogate the imatinib-induced activation of G1 checkpoint and that induction of cell cycle arrest rather than induction of apoptosis was thus the main cause of synergistic growth inhibition in KCL22 and KCL22/SR cells. In contrast, the percentage of G0/G1 cells among K562, KU812, K562/SR or KU812/SR cells was not increased but rather decreased by combination treatment (Fig. 3B). Consistent with these results, the levels of cycline D1 were decreased after combination treatment in K562, KU812, K562/SR and KU812/SR cells (data not shown). The $p27^{KIP1}$ level in KU812/SR cells was slightly increased and maintained for 24 h by treatment with imatinib alone, whereas the level was increased at 6 h but declined afterward in K562, K562/SR and KU812 cells (Fig. 3A). Interestingly, combination treatment with R115777 and imatinib had no inhibitory effect on the imatinib-mediated induction of $p27^{KIP1}$ expression in these cells (Fig. 3A). These results suggest that G0/G1 accumulation was not induced in these cells, unlike in KCL22 and KCL22/SR cells, despite G1 checkpoint activation, probably due to the significant induction of apoptosis after combination treatment.

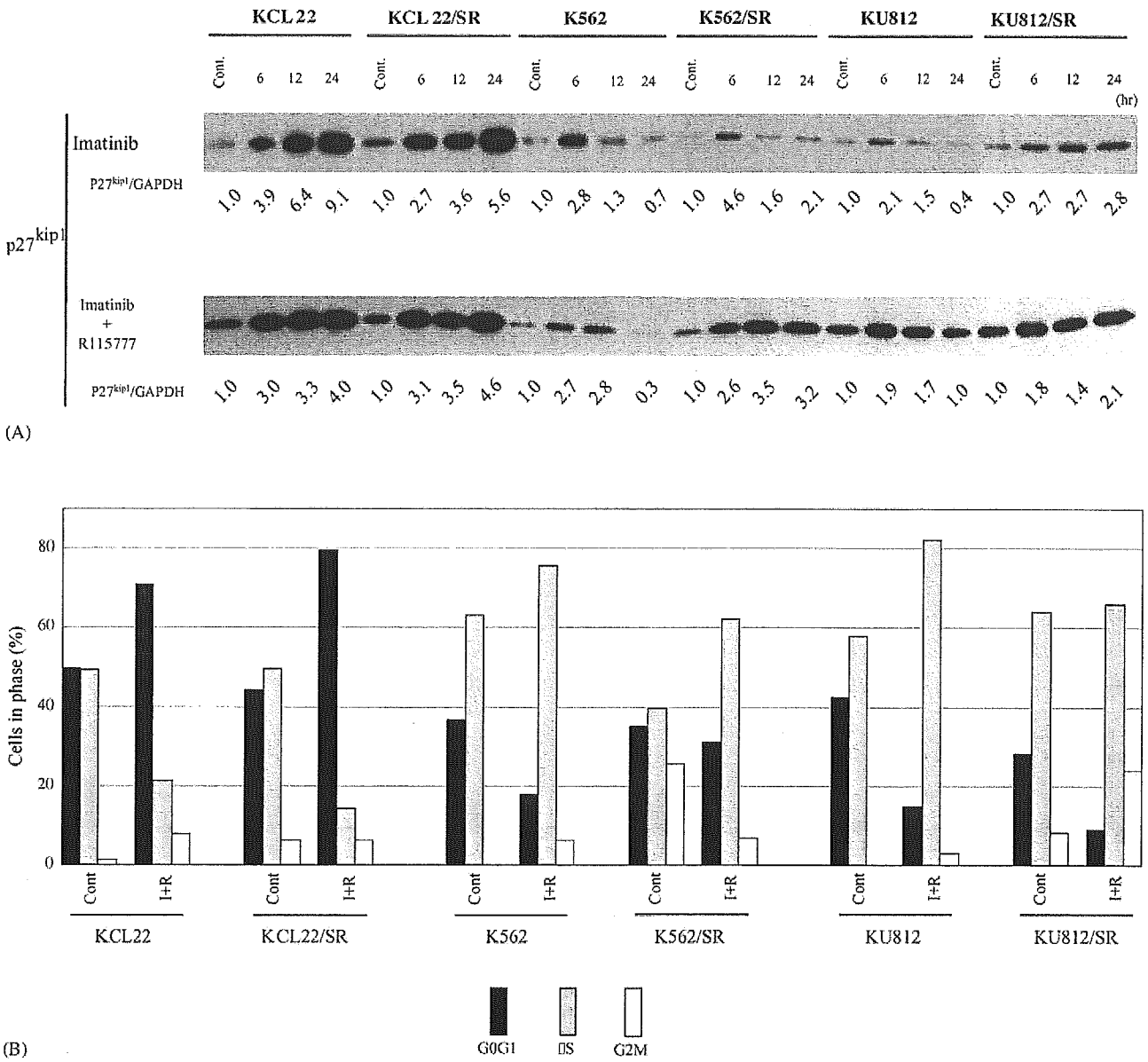

Fig. 3. Effect of combination treatment with R115777 and imatinib on the cell cycle. (A) Changes in $p27^{KIP1}$ protein levels in cells treated with imatinib alone or with a combination of R115777 and imatinib. Cells were cultured in the absence of any reagent for 3 days prior to the treatment and then treated with IC_{50} concentrations of imatinib alone or a combination of IC_{50} concentrations of imatinib and R115777 for 6, 12 and 24 h. Total cell lysates were prepared and subjected to Western blot analysis using anti-$p27^{KIP1}$ antibody. Anti-glyceraldehyde-3-phosphate dehydrogenase (GAPDH) antibody was used as a control for loading (lower panel). (B) Combination treatment of R115777 and imatinib changed the ratios of cell cycle stages. After 24 h of incubation of cells with IC_{50} concentrations of imatinib and R115777, the cells were harvested and incubated with propidium iodide for 30 min and analyzed by flow cytometry with a FACScan/CellFIT system (Becton Dickinson, San Jose, CA).

4. Discussion

Previous studies showed that sustenance of BCR/ABL kinase activity mediated by mechanisms including increased expression of and point mutations in the BCR/ABL gene is a major cause of acquisition of resistance to imatinib [5–14]. In fact, BCR/ABL gene mutations have been found in many clinical imatinib-resistant cases [5–9]. However, there are some cases in which no mutation is found. In the latter cases, deregulation of processes downstream of BCR/ABL kinase may be involved in the resistance to imatinib. Thus, resistance to imatinib can apparently be obtained in both BCR/ABL kinase activity-related and activity-unrelated manners. Imatinib-resistant cell lines examined in the present study exhibited no upregulation of BCR/ABL protein or point mutations in the BCR/ABL gene (data not shown). Moreover, phosphorylation of BCR/ABL was significantly suppressed by imatinib treatment, suggesting that these cells provide a good model of imatinib resistance via a BCR/ABL kinase activity-unrelated mechanism.

FTIs are reagents that may target abnormally activated cellular signaling downstream of BCR/ABL kinase. Previous in vitro studies showed that combinations of FTIs and

imatinib are effective against BCR/ABL-positive cells, but it is unclear whether this effect is additive or synergistic. The present results indicate that combination of R115777 and imatinib synergistically inhibits growth of BCR/ABL-positive cell lines, as indicated by a Steel and Peckham isobologram, which is one of the most reliable methods of analysis for evaluating cell growth inhibition (Fig. 1A). Notably, this synergistic inhibitory effect was also observed in both imatinib-resistant cell lines and leukemia cells from an imatinib-refractory patient (Fig. 1A and B). These results strongly suggest that this combination would have therapeutic value for patients with aggressive BCR/ABL-positive leukemia. It is important to clarify whether the combination treatment is also effective against cells that have resistance-associated mutated BCR/ABL protein, whose kinase activity is not effectively inhibited by imatinib [42]. On the other hand, the contribution of upregulation of P-gp to acquisition of resistance to imatinib is still controversial [43,44]. Fortunately, the effect of the combination treatment may not be influenced by overexpression of P-gp, because the growth of KU812/SR cells (which express P-gp at a level 12.7-fold higher than that in parental KU812 cells) was effectively inhibited by the combination treatment, as was the case with other cell lines.

FTIs were initially developed as inhibitors of posttranslational processing of Ras proteins. However, numerous previous studies suggest that inhibition of the processing of other target proteins such as RhoB, CENP-E and CENP-F is involved in FTI-mediated inhibition of tumor cell proliferation [27,28]. In the present study, R115777 alone had no effect on the levels of phopho-ERK1/2 in any of the BCR/ABL-positive cell lines examined. Taken together with the finding that overexpression of MEK1 (a downstream kinase in the Ras pathway) in KCL22 cells did not restore the cytotoxic effect of the combination treatment (data not shown), this suggests that inhibition of abnormally activated signaling other than Ras-MAPK signaling is involved in synergistic growth inhibition by the combination treatment. We previously found by DNA microarray analyses that RASAP1 and RhoA, which affect or engage in cross talk with cellular signaling, are expressed at higher levels in KCL22/SR cells than in KCL22 cells [36]. It is of interest to clarify whether the effect of the combination treatment is mediated by expression of such molecules.

It has been shown that imatinib induces apoptosis in CML cells [45]. In K562, KU812, K562/SR and KU812/SR cells, R115777 significantly augmented the imatinib-induced increase in the number of annexin-V-positive cells (Fig. 2B). Consistent with these results, the levels of both cleaved caspase 3 and cleaved PARP were increased by the combination treatment. These results suggest that the combination effectively induces apoptosis in these cells. In contrast, the induction of annexin-V-positive cells was extremely low in KCL22 and KCL22/SR cells despite the increase in the level of cleaved caspase 3 by the combination treatment (Fig. 2A and B). One possible explanation for these results is that apoptosis signaling was blocked downstream of caspase 3 in KCL22 and KCL22/SR cells. In fact, the level of cleaved PARP, which is one of the downstream molecules of caspase 3, was much less increased in KCL22 and KCL22/SR cells than in other cell lines (Fig. 2A). Although it is also possible that other unknown mechanisms critically contribute to the blockage of apoptosis, these results suggest that the apoptosis-induction system may break down and that even the combination could not overcome the resistance for the induction of apoptosis in these cells. It is of importance to elucidate the possible unknown mechanisms of apoptosis signaling blockage, and such efforts are now being made in our laboratory.

$p27^{KIP1}$ expression was up-regulated by imatinib alone in all cell lines examined in this study. These results are consistent with our previous findings that imatinib induced cell cycle arrest at the G0/G1 phase, accompanied by up-regulation of $p27^{KIP1}$, in KCL22 cells [46]. Addition of R115777 resulted in no suppression of imatinib-induced up-regulation of $p27^{KIP1}$ expression in all cell lines, suggesting that the combination could not inhibit imatinib-dependent activation of the G1 checkpoint. It is noteworthy that R115777 alone increased the $p27^{KIP1}$ level (in K562, KU812, KCL22 and KCL22/SR cells) or had no effect on the $p27^{KIP1}$ level (in K562/SR and KU812/SR cells) (data not shown). Since FTIs have been shown to induce cell cycle arrest via inhibition of farnesylation of CENP-E protein [47,48], it is possible that CENP-E was a target molecule of R115777 in these cells. Since the apoptosis signal was blocked downstream of caspase 3, the percentage of G0/G1 cells was significantly increased with G1 checkpoint activation after the combination treatment in KCL22 and KCL22/SR cells (Fig. 3A and B). Therefore, it is concluded that cell cycle blockage was mainly involved in the synergistic cell growth inhibition by the combination treatment in KCL22 and KCL22/SR cells. We previously showed that treatment of KCL22 cells with 20 μM imatinib also resulted in G0/G1 accumulation but not in induction of apoptosis [46]. In this study, combined treatment of KCL22 and KCL22/SR cells with R115777 and a higher concentration (5 μM) of imatinib also resulted in G0/G1 accumulation (data not shown). These results suggest that a high concentration of imatinib could not overcome G1 checkpoint activation in these cells.

The other cell lines, K562, KU812, K562/SR and KU812/SR, exhibited different responses. Although the level of $p27^{KIP1}$ was increased by the combined treatment, the percentage of G0/G1 cells was not increased but was rather decreased. The reason for these discrepant phenomena may be the significant induction of apoptosis in these cells. It is likely that apoptosis is induced in the cells before they are led to a G0/G1 state. These results suggest that the induction of apoptosis but not cell cycle blockage plays an important role in the synergistic growth inhibition of K562,

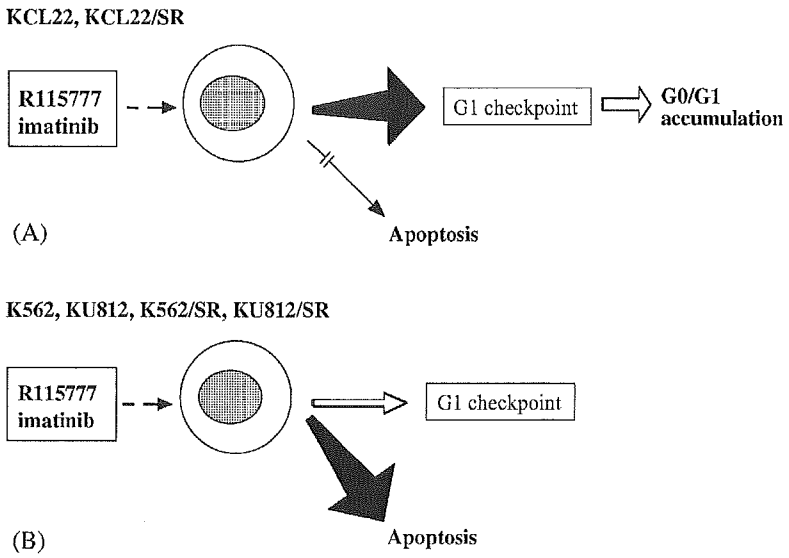

Fig. 4. Hypothetical scheme of the different responses to the combination of R115777 and imatinib in BCR/ABL-positive cells. (A) The combination treatment activates the G1 checkpoint, leading to G0/G1-phase accumulation in KCL22 and KCL22/SR cells, in which apoptosis signaling breaks down. (B) K562, KU812, K562/SR and KU812/SR cells undergo apoptosis with the combination treatment without induction of G0/G1 accumulation.

KU812, K562/SR and KU812/SR cells. A model for the different responses to the combination treatment is presented in Fig. 4. This predicts that the G1 checkpoint remains active but apoptosis signaling breaks down under the condition of combination treatment, leading to G0/G1-phase accumulation in KCL22 and KCL22/SR cells. In contrast, K562, KU812, K562/SR and KU812/SR cells mainly undergo apoptosis by the combination treatment. It is interesting that the imatinib-resistant clone and each corresponding parental cell line showed similar responses to the combination treatment. Therefore, the different pattern of responses might be due to some original cell characteristics, which remain even after acquisition of resistance to imatinib.

The results of this study suggest that the combination treatment of R115777 and imatinib effectively reduce the number of leukemia cells regardless of the sensitivity to imatinib. The finding that the relative importance of the two major mechanisms involved in synergistic inhibition, induction of apoptosis and cell cycle blockage, differed among cell types may have important implications for clinical application of the combination treatment. Since primitive, quiescent BCR/ABL-positive cells may be resistant to imatinib [49], it is likely that KCL22 or KCL22/SR-type leukemia cells, the cell cycles of which are induced to a standstill, may survive after the combination treatment and grow later in the clinical course. Therefore, additional treatment for overriding the G1 checkpoint may be required to eradicate these types of leukemia cells.

Acknowledgments

We are grateful to Drs. Y. Furukawa, T. Kondo, S. Nakano and K. Mitsugi for their helpful discussions. We also thank Ms. E. Yamakawa for her help in preparation of the manuscript. This work was supported by grants-in-aid from the Ministry of Education, Culture, Sports, Science and Technology, Japan.

References

[1] Kantarjian H, Sawyers C, Hochhaus A, Guilhot F, Schiffer C, Gambacorti-Passerini C, et al. Hematologic and cytogenetic responses to imatinib mesylate in chronic myelogenous leukemia. N Engl J Med 2002;346:645–52.
[2] Hughes TP, Kaeda J, Branford S, Rudzki Z, Hochhaus A, Hensley ML, et al. Frequency of major molecular responses to imatinib or interferon alfa plus cytarabine in newly diagnosed chronic myeloid leukemia. N Engl J Med 2003;349:1423–32.
[3] Sawyers CL, Hochhaus A, Feldman E, Goldman JM, Miller CB, Ottmann OG, et al. Imatinib induces hematologic and cytogenetic responses in patients with chronic myelogenous leukemia in myeloid blast crisis: results of a phase II study. Blood 2002;99:3530–9.
[4] Druker BJ, Sawyers CL, Kantarjian H, Resta DJ, Reese SF, Ford JM, et al. Activity of a specific inhibitor of the BCR/ABL tyrosine kinase in the blast crisis of chronic myeloid leukemia and acute lymphoblastic leukemia with the Philadelphia chromosome. N Engl J Med 2001; 344:1038–42.
[5] Shah NP, Nicoll JM, Nagar B, Gorre ME, Paquette RL, Kuriyan J, et al. Multiple BCR-ABL kinase domain mutations confer polyclonal resistance to the tyrosine kinase inhibitor imatinib (STI571) in chronic phase and blast crisis chronic myeloid leukemia. Cancer Cell 2002; 2:117–25.
[6] Gorre ME, Mohammed M, Ellwood K, Hsu N, Paquette R, Rao PN, et al. Clinical resistance to STI571 cancer therapy caused by BCR-ABL gene mutation of amplification. Science 2001;293:876–80.
[7] Branford S, Rudzki Z, Walsh S, Grigg A, Arthur C, Taylor K, et al. High frequency of point mutations clustered within the adenosine triphosphate-binding region of BCR/ABL in patients with chronic myeloid leukemia or Ph-positive acute lymphoblastic leukemia who develop imatinib (STI571) resistance. Blood 2002;99:3472–5.
[8] von Bubnoff N, Schneller F, Peschel C, Duyster J. BCR-ABL gene mutations in relation to clinical resistance of Philadelphia-chromo-

some-positive leukemia to STI571: a prospective study. Lancet 2002;359:487–91.
[9] Ricci C, Scappini B, Divoky V, Gatto S, Onida F, Verstovsek S, et al. Mutation in the ATP-binding pocket of the ABL kinase domain in an STI571-resistant BCR/ABL-positive cell line. Cancer Res 2002; 62:5995–8.
[10] le Coutre P, Tassi E, Varella-Garcia M, Barni R, Mologni L, Cabrita G, et al. Induction of resistance to the Abelson inhibitor STI571 in human leukemic cells through gene amplification. Blood 2000;95:1758–66.
[11] Weisberg E, Griffin JD. Mechanism of resistance to the ABL tyrosine kinase inhibitor STI571 in BCR/ABL-transformed hematopoietic cell lines. Blood 2000;95:3498–505.
[12] Mahon FX, Deininger MW, Schultheis B, Chabrol J, Reiffers J, Goldman JM, et al. Selection and characterization of BCR-ABL positive cell lines with differential sensitivity to the tyrosine kinase inhibitor STI571: diverse mechanisms of resistance. Blood 2000; 96:1070–9.
[13] Gambacorti-Passerini C, Barni R, le Coutre P, Zucchetti M, Cabrita G, Cleris L, et al. Role of α1 acid glycoprotein in the in vivo resistance of human BCR-ABL$^+$ leukemic cells to the Abl inhibitor STI571. J Natl Cancer Inst 2000;92:1641–50.
[14] Tarumoto T, Nagai T, Ohmine K, Miyoshi T, Nakamura M, Kondo T, et al. Ascorbic acid restores the sensitivity to imatinib through suppression of Nrf2-dependent gene expression in a imatinib-resistant cell line, KCL22/SR. Exp Hematol 2004;32:375–81.
[15] Roche-Lestienne C, Soenen-Cornu V, Grardel-Duflos N, Lai JL, Philippe N, Facon T, et al. Several types of mutations of the Abl gene can be found in chronic myeloid leukemia patients resistant to STI571, and they can pre-exist to the onset of treatment. Blood 2002;100:1014–8.
[16] Kreuzer KA, Le Coutre P, Landt O, Na IK, Schwarz M, Schultheis K, et al. Preexistence and evolution of imatinib mesylate-resistant clones in chronic myelogenous leukemia detected by a PNA-based PCR clamping technique. Ann Hematol 2003;82:284–9.
[17] Hofmann WK, Komor M, Wassmann B, Jones LC, Gschaidmeier H, Hoelzer D, et al. Presence of the BCR-ABL mutation Glu255Lys prior to STI571 (imatinib) treatment in patients with Ph+ acute lymphoblastic leukemia. Blood 2003;102:659–61.
[18] La Rosee P, Corbin AS, Stoffregen EP, Deininger MW, Druker BJ. Activity of the Bcr-Abl kinase inhibitor PD180970 against clinically relevant Bcr-Abl isoforms that cause resistance to imatinib mesylate (Gleevec, STI571). Cancer Res 2002;62:7149–53.
[19] Mow BM, Chandra J, Svingen PA, Hallgren CG, Weisberg E, Kottke TJ, et al. Effects of the Bcr/abl kinase inhibitors STI571 and adaphostin (NSC 680410) on chronic myelogenous leukemia cells in vitro. Blood 2002;99:664–71.
[20] Nagar B, Bornmann WG, Pellicena P, Schindler T, Veach DR, Miller WT, et al. Crystal structures of the kinase domain of c-Abl in complex with the small molecule inhibitors PD173955 and imatinib (STI-571). Cancer Res 2002;62:4236–43.
[21] Wisniewski D, Lambek CL, Liu C, Strife A, Veach DR, Nagar B, et al. Characterization of potent inhibitors of the Bcr-Abl and the c-kit receptor tyrosine kinases. Cancer Res 2002;62:4244–55.
[22] Tipping AJ, Melo JV. Imatinib mesylate in combination with other chemotherapeutic drugs: in vitro studies. Semin Hematol 2003; 40(Suppl. 2):83–91.
[23] Druker BJ. Overcoming resistance to imatinib by combining targeted agents. Mol Cancer Ther 2003;2:225–6.
[24] Rowinsky EK, Windle JJ, Von Hoff DD. Ras protein farnesyltransferase: a strategic target for anticancer therapeutic development. J Clin Oncol 1999;17:3631–52.
[25] Gibbs RA. Farnesyltransferase inhibitors: novel anticancer mechanisms and new therapeutic applications. Curr Opin Drug Dis Dev 2000;3:585–96.
[26] Kohl NE, Omer CA, Conner MW, Anthony NJ, Davide JP, deSolms SJ, et al. Inhibition of farnesyltransferase induces regression of mammary and salivary carcinomas in ras transgenic mice. Nat Med 1995;1: 792–7.
[27] Ashar HR, James L, Gray K, Carr D, Black S, Armstrong L, et al. Farnesyl transferase inhibitors block the farnesylation of CENP-E and CENP-F and alter the association of CENP-E with the microtubules. J Biol Chem 2000;275:30451–7.
[28] Lebowitz PF, Prendergast GC. Non-Ras targets of farnesyltransferase inhibitors: focus on Rho. Oncogene 1998;17:1439–45.
[29] Peters DG, Hoover RR, Gerlach MJ, Koh EY, Zhang H, Choe K, et al. Activity of the farnesyl protein transferase inhibitor SCH66336 against BCR/ABL-induced murine leukemia and primary cells from patients with chronic myeloid leukemia. Blood 2001;97:1404–12.
[30] Reichert A, Heisterkamp N, Daley GQ, Groffen J. Treatment of Bcr/Abl-positive acute lymphoblastic leukemia in P190 transgenic mice with the farnesyl transferase inhibitor SCH66336. Blood 2001; 97:1399–403.
[31] Hoover RR, Mahon FX, Melo JV, Daley GQ. Overcoming STI571 resistance with the farnesyl transferase inhibitor SCH66336. Blood 2002;100:1068–71.
[32] Karp JE, Lancet JE, Kaufmann SH, End DW, Wright JJ, Bol K, et al. Clinical and biologic activity of the farnesyltransferase inhibitor R115777 in adults with refractory and relapsed acute leukemias: a phase 1 clinical-laboratory correlative trial. Blood 2001;97:3361–9.
[33] Cortes J, Albitar M, Thomas D, Giles F, Kurzrock R, Thibault A, et al. Efficacy of the farnesyl transferase inhibitor R115777 in chronic myeloid leukemia and other hematologic malignancies. Blood 2003;101:1692–7.
[34] Cortes J, Garcia-Manero G, O'Brien S, Hernandez I, Rackoff W, Faderl S, et al. Phase I study of a imatinib and Tipifarnib (Zarnestra^{TM}, R115777) in patients with chronic myeloid leukemia in chronic phase refractory to imatinib. Blood 2003;102:909a.
[35] Gotlib J, Mauro M, O'Dwyer ME, Fechter L, Dugan K, Kuyl J, et al. Tipifarnib (Zarnestra^{TM}) and imatinib (Gleevec^{TM}) combination therapy in patients with advanced chronic myelogenous leukemia (CML): preliminary results of a phase I study. Blood 2003;102:909a.
[36] Ohmine K, Nagai T, Tarumoto T, Miyoshi T, Muroi K, Mano H, et al. Analysis of gene expression profiles in an imatinib-resistant cell line, KCL22/SR. Stem Cells 2003;21:315–21.
[37] Steel GG, Peckham MJ. Exploitable mechanisms in combined radiotherapy-chemotherapy: the concept of additivity. Int J Radiat Oncol Biol Phys 1979;5:85–91.
[38] Kano Y, Akutsu M, Tsunoda S, Mano H, Sato Y, Honma Y, et al. In vitro cytotoxic effects of a tyrosine kinase inhibitor STI571 in combination with commonly used antileukemic agents. Blood 2001;97: 1999–2007.
[39] Lassar AB, Davis RL, Wright WE, Kadesch T, Murre C, Voronova A, et al. Functional activity of myogenic HLH proteins requires hetero-oligomerization with E12/E47-like proteins in vivo. Cell 1991; 66:305–15.
[40] Nagai T, Harigae H, Ishihara H, Motohashi H, Minegishi N, Tsuchiya S, et al. Transcription factor GATA-2 is expressed in erythroid, early myeloid, and CD34+ human leukemia-derived cell lines. Blood 1994;84:1074–84.
[41] Adjei AA, Davis JN, Erlichman C, Svingen PA, Kaufmann SH. Comparison of potential markers of farnesyltransferase inhibition. Clin Cancer Res 2000;6:2318–25.
[42] Hochhaus A. Cytogenetic and molecular mechanisms of resistance to imatinib. Semin Hematol 2003;40:69–79.
[43] Mahon FX, Belloc F, Lagarde V, Chollet C, Moreau-Gaudry F, Reiffers J, et al. MDR1 gene overexpression confers resistance to imatinib mesylate in leukemia cell line models. Blood 2003; 101:2368–73.
[44] Ferrao PT, Frost MJ, Siah SP, Ashman LK. Overexpression of P-glycoprotein in K562 cells does not confer resistance to the growth inhibitory effects of imatinib (STI571) in vitro. Blood 2003;102: 4499–503.

[45] Jacquel A, Herrant M, Legros L, Belhacene N, Luciano F, Pages G, et al. Imatinib induces mitochondria-dependent apoptosis of the Bcr-Abl-positive K562 cell line and its differentiation towards the erythroid lineage. FASEB J 2003;17:2160–2.
[46] Komatsu N, Watanabe T, Uchida M, Mori M, Kirito K, Kikuchi S, et al. A member of Forkhead transcription factor FKHRL1 is a downstream effector of STI571-induced cell cycle arrest in BCR-ABL-expressing cells. J Biol Chem 2003;278:6411–9.
[47] Ashar HR, James L, Gray K, Carr D, Black S, Armstrong L, et al. Farnesyl transferase inhibitors block the farnesylation of CENP-E and CENP-F and alter the association of CENP-E with the microtubules. J Biol Chem 2000;275:30451–7.
[48] Ashar HR, James L, Gray K, Carr D, McGuirk M, Maxwell E, et al. The farnesyl transferase inhibitor SCH 66336 induces a G(2) → M or G(1) pause in sensitive human tumor cell lines. Exp Cell Res 2001; 262:17–27.
[49] Graham SM, Jorgensen HG, Allan E, Pearson C, Alcorn MJ, Richmond L, et al. Primitive, quiescent, Philadelphia-positive stem cells from patients with chronic myeloid leukemia are insensitive to STI571 in vitro. Blood 2002;99:319–25.

STEM CELLS®
Original Article

Repair of Infarcted Myocardium Mediated by Transplanted Bone Marrow–Derived CD34+ Stem Cells in a Nonhuman Primate Model

TORU YOSHIOKA[a,c] NAOHIDE AGEYAMA,[f] HIROAKI SHIBATA,[a,f] TAKANORI YASU,[c] YOSHIO MISAWA,[d] KOICHI TAKEUCHI,[e] KEIJI MATSUI,[c] KEIJI YAMAMOTO,[c] KEIJI TERAO,[f] KAZUYUKI SHIMADA,[c] UICHI IKEDA,[g] KEIYA OZAWA,[a,b] YUTAKA HANAZONO[a]

[a]Center for Molecular Medicine; [b]Division of Hematology, and [c]Division of Cardiology, Department of Internal Medicine; [d]Division of Cardiovascular Surgery, Department of Surgery; and [e]Department of Anatomy, Jichi Medical School, Minamikawachi, Tochigi; [f]Tsukuba Primate Center, National Institute of Infectious Diseases, Tsukuba, Ibaraki; [g]Department of Organ Regeneration, Shinshu University Graduate School of Medicine, Matsumoto, Nagano, Japan

Key Words. Nonhuman primate • Acute myocardial infarction • Stem cell transplantation Genetic marking • Lentivirus vector • Plasticity • Neoangiogenesis

ABSTRACT

Rodent and human clinical studies have shown that transplantation of bone marrow stem cells to the ischemic myocardium results in improved cardiac function. In this study, cynomolgus monkey acute myocardial infarction was generated by ligating the left anterior descending artery, and autologous CD34+ cells were transplanted to the peri-ischemic zone. To track the in vivo fate of transplanted cells, CD34+ cells were genetically marked with green fluorescent protein (GFP) using a lentivirus vector before transplantation (marking efficiency, 41% on average). The group receiving cells ($n = 4$) demonstrated improved regional blood flow and cardiac function compared with the saline-treated group ($n = 4$) at 2 weeks after transplant. However, very few transplanted cell–derived, GFP-positive cells were found incorporated into the vascular structure, and GFP-positive cardiomyocytes were not detected in the repaired tissue. On the other hand, cultured CD34+ cells were found to secrete vascular endothelial growth factor (VEGF), and the in vivo regional VEGF levels showed a significant increase after the transplantation. These results suggest that the improvement is not the result of generation of transplanted cell–derived endothelial cells or cardiomyocytes; and raise the possibility that angiogenic cytokines secreted from transplanted cells potentiate angiogenic activity of endogenous cells.
STEM CELLS *2005;23:355–364*

INTRODUCTION

Recent clinical studies have shown that the introduction of bone marrow cells can restore blood flow in ischemic myocardium and ameliorate cardiac function [1–6]. Despite enthusiasm for these studies, it is unclear how transplanted bone marrow cells contribute to the clinical improvement. Because endothelial progenitor cells are identified in bone marrow cells [7], these cells might participate in the repair

Correspondence: Yutaka Hanazono, M.D., Ph.D., Division of Regenerative Medicine, Center for Molecular Medicine, Jichi Medical School, 3311-1 Yakushiji, Minamikawachi, Tochigi 329-0498, Japan. Telephone: 81-285-58-7450; Fax: 81-285-44-5205; e-mail: hanazono@jichi.ac.jp Received August 16, 2004; accepted for publication November 30, 2004. 1066-5099/2005/$12.00/0 doi: 10.1634/stemcells.2004-0200

of vascular tissue. On the other hand, it has been reported that hematopoietic stem cells differentiate into endothelial cells and cardiomyocytes when transplanted into the ischemic myocardium in mice [8]. More recently, however, it has been reported that hematopoietic stem cells do not give rise to nonhematopoietic cells in the ischemic myocardium in murine models [9–11].

In vivo tracking and plastic properties of hematopoietic stem or progenitor cells have not been examined in primate cardiac ischemia. We have transplanted genetically marked autologous CD34+ cells to the ischemic myocardium in a nonhuman primate (cynomolgus macaque) model and tracked the in vivo fate of the cells. We have used CD34+ cells because the cells are widely used as a fraction of hematopoietic stem cells in clinical and nonhuman primate studies [12]. In addition, CD34+ cells contain vascular endothelial progenitor cells [7]. Thus, the present study can address the question of whether transplanted CD34+ cells really give rise to endothelial cells and cardiomyocytes in ischemic myocardium in primates.

Materials and Methods

Animals

Eight cynomolgus macaques bred in the Tsukuba Primate Center (Ibaraki, Japan) were enrolled in the present study. This study strictly adhered to the rules for animal care and management of the Tsukuba Primate Center, as well as the guiding principles for animal experiments using nonhuman primates formulated by the Primate Society of Japan. The protocols of animal experiments were approved by the animal welfare and animal care committee of the National Institute of Infectious Diseases (Tokyo).

Preparation of CD34+ Cells

Cynomolgus bone marrow (50 ml) was aspirated from the iliac crest under an isoflurane-induced general anesthesia. From the bone marrow, a nucleated cell fraction was obtained after red blood cell lysis with addition of ACK buffer (Biosource, Camarillo, CA). CD34+ cells were isolated using magnetic beads conjugated with anti-human CD34 (clone 561; Dynal, Lake Success, NY), which cross-reacts with cynomolgus CD34 [13]. The purity of CD34+ cells at harvest ranged from 90% to 95%, as assessed with another anti-human CD34 (clone 563; PharMingen, San Diego) that cross-reacts with cynomolgus CD34 [13]. The purity remained at the same levels after the 1-day transduction culture, which is discussed next.

Lentiviral Transduction

A simian immunodeficiency virus (SIV)-based lentivirus vector carrying enhanced jellyfish green fluorescent protein (GFP) (Clontech, Palo Alto, CA) was used for transduction. The vector was prepared as previously reported [14, 15]. All recombinant DNA experiments were approved by the Ministry of Education, Culture, Sports, Science and Technology of Japan.

CD34+ cells (1×10^6) were seeded in six-well plates in 2 ml of StemSpan serum-free expansion medium (Stem Cell Technologies, Vancouver) supplemented with recombinant human thrombopoietin (100 ng/ml; Kirin, Tokyo), recombinant human stem cell factor (100 ng/ml; Biosource, Camarillo, CA), recombinant human Flt-3 ligand (100 ng/ml; Research Diagnostics, Flanders, NJ), and antibiotics (100 U/ml of penicillin and 0.1 μg/ml of streptomycin; Meiji, Tokyo). The cells were transduced twice each for 12 hours (total, 24 hours) with the SIV vector at 50 transducing units per target cell. After transduction, cells were cryopreserved with 10% dimethylsulfoxide (Wako, Osaka, Japan) and 1% Dextran 40 (Yoshitomi, Osaka, Japan) in a controlled-rate programmable freezer (Kryo 10; Planer Biomed, Middlesex, UK) until transplantation. The viability of cells after thawing was 53.0 ± 6.5%, as assessed by trypan blue staining. An aliquot of transduced cells was assessed for GFP expression at 48 hours after transduction by flow cytometry using a FACScan (Becton Dickinson, Franklin Lakes, NJ) with excitation at 488 nm and fluorescence detection at 530 ± 30 nm.

In Vitro Endothelial Differentiation

CD34+ cells were seeded on fibronectin-coated plates (Becton Dickinson) in M199 medium (Invitrogen, Carlsbad, CA) with 20% fetal calf serum and bovine pituitary extracts (Invitrogen) as previously described [7]. After 7 days in culture, cells were examined for the uptake of DiI-acetylated low-density lipoprotein (LDL) and for the expression of CD31, von Willebrand factor (vWF), vascular endothelial (VE)-cadherin, and vascular endothelial growth factor receptor (VEGFR)-2. Briefly, adherent cells were incubated with 1 μg/ml of DiI-acetylated LDL (Molecular Probes, Eugene, OR) for 4 hours at 37°C. For immunofluorescence staining, after fixation in ice-cold 4% paraformaldehyde for 10 minutes and blocking in 1% bovine serum albumin (BSA) for 15 minutes, cells were incubated with a primary antibody: mouse anti-human CD31 (VM-59; Becton Dickinson), rabbit anti-human vWF (DakoCytomation, Glostrup, Denmark), mouse anti-human VE-cadherin (55-7H1; Becton Dickinson), or rabbit anti-mouse VEGFR2 (Santa Cruz Biotechnology, Santa Cruz, CA) for 1 hour at room

temperature. Cells were then incubated with a secondary antibody, Texas red–conjugated horse anti-mouse immunoglobulin G (IgG) (Vector, Burlingame, CA) or goat anti-rabbit IgG (Vector) for 30 minutes at room temperature.

Myocardial Infarction and Transplantation

All operations on cynomolgus monkeys were performed under an isoflurane-induced general anesthesia. Thoracotomy was conducted, the pericardium was opened, and the left anterior descending coronary artery was ligated with 5-0 prolene sutures. One to 2 hours after the ligation, GFP-transduced, autologous $CD34^+$ cells in normal saline were injected with a microsyringe through a 27-gauge needle into 10 sites (5 μl/site) in the peri-ischemic zone. In the control group, saline alone was injected in the same way. The pericardium and chest were closed. The animals then received butorphanol tartrate (0.5 mg/kg, intramuscularly) daily for 5 days to alleviate the pain associated with the operation and myocardial infarction.

Echocardiography

Echocardiographic imaging was obtained using a Sonos 5500 system (Philips Medical Systems, Andover, MA) before transplantation and at 2 weeks after transplant. The echocardiography was conducted by independent technicians irrelevant to our study group. In one animal (BM97080), it was additionally performed at 12 weeks. Short-axis two-dimensional images at the midpapillary level of the left ventricle were stored, and percent fractional shortening (%FS) was calculated to assess cardiac function.

Myocardial contrast echocardiography (MCE) was performed at day 0 (just before transplantation) and at 2 weeks after transplant to assess regional blood flow and blood flow defect size. In one animal (BM97080), chronic assessment was performed at 12 weeks after transplant. The electrocardiograph-triggered end-systolic intermittent imaging was conducted in short-axis views at incremental pulsing intervals (triggering intervals of 1, 2, 3, 4, and 8 beats) using an S12 probe. Once optimized, the settings of depth (4 cm), mechanical index (0.9), and focus (3 cm) were fixed. The contrast agent (perflutren; Yamanouchi, Tokyo) consisted of lipid-coated microbubbles of perfluorocarbon [16]. Perflutren diluted with saline (1:10) was administered intravenously at a constant rate (0.01 ml/kg per min). For the assessment of regional blood flow, MCE images were analyzed using ORIGIN 6.0J (Lightstone, Tokyo), and the blood flow was calculated as previously described [17]. Data are presented as a blood flow ratio (the peri-infarct versus nonischemic control region or the infarct versus nonischemic control region). For the assessment of blood flow defect, MCE images obtained at triggering interval of four beats were analyzed using National Institutes of Health Image software (version 1.61). Data are presented as percent defect compared with the total blood flow.

Microspheres

Colored microspheres (15 μm ± 2% diameter; E-Z Trac, Los Angeles) were used to evaluate regional blood flow 2 weeks after transplant [18], with the exception of one animal (BM97080), in which evaluation was performed 12 weeks after transplant. A set of microspheres (2×10^6) was diluted in 2 ml of saline and injected into the left ventricle over 30 seconds. A reference blood sample was withdrawn at a constant rate of 5 ml/min through the femoral artery. After the collection of blood samples, monkeys were irrigated with saline for mercy killing and blood was completely washed out. The heart was excised from each monkey. Tissue samples from the infarct, peri-infarct, and nonischemic regions (one sample per region) were digested, microspheres were collected, and the blood flow was calculated according to the manufacturer's instructions. Data are presented as blood flow ratio (the peri-infarct versus nonischemic control region or the infarct versus nonischemic control region).

Immunohistochemistry

Tissue samples from the infarct, peri-infarct, and nonischemic regions at 2 weeks after transplant were embedded in optimal cutting temperature compound (Sakura, Zoeterwoude, Netherlands) and frozen in liquid nitrogen. Sections were prepared (6 μm), fixed for 10 minutes at 4°C in 4% paraformaldehyde in phosphate-buffered saline (PBS), and blocked with 1% BSA in PBS. The sections were incubated at room temperature with a primary antibody, monoclonal mouse anti-human CD31 (1:200; Becton Dickinson), followed by a secondary antibody, biotin-conjugated horse anti-mouse IgG (1:500; Vector). The sections were then treated with avidin-alkaline phosphatase (ABC AP kit; Vector) for 30 minutes. The reaction was developed with a Vector Red substrate kit (SK-5100; Vector). In the case of double staining of CD31 and GFP, the above sections were further incubated with polyclonal rabbit anti-GFP (1:200; Clontech) followed by biotin-conjugated anti-rabbit IgG (1:500; Vector) and treated with avidin-peroxidase (ABC Elite kit; Vector). The reaction was developed with a Vector SG substrate kit (SK-4700; Vector). The sections were counterstained with hematoxylin, mounted in glycerol, and examined under a light microscope.

In Situ Polymerase Chain Reaction

In situ detection of transduced cell progeny was performed by amplifying proviral sequences as previously reported [19]. The following primer set for the GFP gene was used:

5'-CGT CCA GGA GCG CAC CAT CTT C-3' and 5'-GGT CTT TGC TCA GGG CGG ACT-3'. The polymerase chain reaction (PCR) mixture consisted of 420 μM dATP, 420 μM dCTP, 420 μM dGTP, 378 μM dTTP, 42 μM digoxigenin-labeled dUTP (Roche, Mannheim, Germany), 0.8 μM of each GFP primer, 4.5 mM $MgCl_2$, 1 × PCR buffer (Mg^{2+} free), and 4 U of Takara Taq DNA polymerase (Takara, Kyote). Sections were prepared with a Takara slide frame (Takara) from the infarct, peri-infarct, and nonischemic regions at 2 weeks after transplant. PCR was performed using a PTC100 thermal cycler (MJ Research, Watertown, MA) with the following conditions: 94°C for 1 minute and 57°C for 1 minute with 10 cycles. The digoxigenin-incorporated DNA fragments were detected using horseradish peroxidase (HRP)-conjugated rabbit F(ab') anti-digoxigenin antibody (DakoCytomation). The sections were then stained for HRP using a Vector SG substrate kit (Vector). Finally, the sections were counterstained with a Kernechtrot solution (Muto, Tokyo) that stains nucleotides, mounted in glycerol, and examined under a light microscope.

ELISA

Vascular endothelial growth factor (VEGF) and basic fibroblast growth factor (bFGF) levels in tissue lysate or medium were assessed by ELISA (R&D Systems, Minneapolis) according to the manufacturer's instructions. Tissue lysate was obtained from the peri-infarct region (three samples from each monkey) at 2 weeks after transplant. Briefly, tissue was homogenized and suspended in lysis buffer containing 10 mM Tris-HCl (pH 8.0), 1% Nonidet P-40, 150 mM NaCl, and protease inhibitor cocktail tablets (Complete Mini, Roche). The suspension was rocked at 4°C for 20 minutes and centrifuged at 16,000g and 4°C for 30 minutes. The supernatant was used for ELISA. The protein concentration of lysate was determined with DC Protein Assay (Bio-Rad, Hercules, CA).

Results

Lentiviral Marking

The CD34+ fraction of autologous bone marrow cells was used for transplantation in our study (Table 1). Before transplantation, CD34+ cells were genetically marked with GFP using an SIV-based lentivirus vector. The ex vivo transduction results are summarized in Table 1. The transduced cells were frozen until transplantation. An aliquot of the transduced cells was examined in vitro for the endothelial differentiation ability. After the differentiation culture, a vessel-like structure was observed (Fig. 1A). The ability of cells to take up DiI-acetylated LDL and the expression of CD31, vWF, VE-cadherin, and VEGFR-2 suggested the endothelial lineage (Fig. 1B). We and others have already confirmed the ability of hematopoietic differentiation of the cells [20, 21]. Taken together, the SIV-mediated GFP gene transfer does not spoil the differentiation abilities of CD34+ cells. In addition, on average, 41% of cells fluoresced 48 hours after transduction, and 56% of

Table 1. Summary of ex vivo transduction and transplantation

	Sex	Age (y)	Body weight (kg)	Harvested bone marrow cell number	Isolated CD34+ cell number	Transplanted cell number	% GFP expression Before[a]	% GFP expression After[b]
Saline group								
CTR01061[c]	M	3	4.1			NA		
CTR99056	M	3	3.4					
CTR96116	F	5	3.2					
CTR99051	M	5	5.9					
CD34+ cell group								
BM01052	M	3	3.9	213×10^6	1.00×10^6	0.47×10^6	49	87
BM01051[d]	M	3	4.1	396×10^6	5.14×10^6	2.20×10^6	51	54
BM97080[e]	M	5	3.9	330×10^6	2.35×10^6	1.04×10^6	49	67
BM90047	M	13	5.8	343×10^6	3.10×10^6	1.07×10^6	16	14
Average		5	4.3	321×10^6	2.90×10^6	1.20×10^6	41	56

[a]Before endothelial differentiation of GFP-transduced CD34+ cells.
[b]After the in vitro endothelial differentiation.
[c]CTR01061 died of heart failure 5 days after myocardial infarction.
[d]BM01051 developed a ventricular aneurysm after myocardial infarction.
[e]BM97080 was killed 12 weeks after the treatment. All other animals were killed 2 weeks after the treatment.
Abbreviations: GFP, green fluorescent protein; NA, not applicable.

endothelial cells still fluoresced after in vitro differentiation (Table 1), showing that the GFP expression is stable during the in vitro differentiation to endothelial cells. Thus, GFP was expected to serve as a good genetic tag after transplantation.

Acute Myocardial Infarction and Autologous Transplantation

Cynomolgus acute myocardial infarction was generated by ligating the left anterior descending artery. One to two hours after the ligation, GFP-transduced, autologous CD34$^+$ cells were injected in the peri-ischemic zone at 10 sites (total, $1.20 \pm 0.73 \times 10^6$ cells; $n = 4$). In the control group, saline was injected in the same way ($n = 4$). We conducted contrast echocardiography immediately after the coronary ligation and found no significant differences in the blood flow defect size (percent blood flow defect compared with the total) between the cell-treated and saline-treated groups ($13.0 \pm 2.1\%$ versus $12.3 \pm 3.5\%$, $p = .75$), suggesting that the initial risk of infarction did not differ between the two groups. In addition, we tried to assess the cardiac isozyme of serum creatine kinase (CK) to evaluate the infarct size; however, either the immuno-inhibition assay or chemical luminescence immunoassay did not work well for cynomolgus monkey samples. We were at least able to show that total CK values at 24 hours after the ligation did not significantly differ between the two groups ($p = .83$).

One of the control monkeys (CTR01061) died of heart failure 5 days after myocardial infarction, and the other control monkeys showed a decrease in %FS at 2 weeks after infarction (Fig. 2). Thus, all four control animals showed the deteriorated cardiac function. In the cell-treated group, one monkey (*, BM01051) underwent ventricular fibrillation immediately after the ligation and survived after cardiopulmonary resuscitation but eventually developed a ventricular aneurysm. Only this animal showed a decrease in %FS despite CD34$^+$ cell treatment; the other animals receiving CD34$^+$ cells showed an increase in %FS (Fig. 2). CD34$^+$ cell treatment may not be able to rescue such a heavily impaired heart but otherwise had a significant effect on cardiac function. Even an old monkey (BM90047, Table 1) showed improved %FS.

The relative blood flow in the peri-infarct to nonischemic control region was also significantly ameliorated in the CD34$^+$ cell–treated monkeys compared with the saline-treated ones, as assessed using contrast echocardiography (Fig. 3A) and colored microspheres (Fig. 3B). An excellent correlation was found between the two methods (Fig. 3C; correlation coefficient = 0.93). Two groups (CD34$^+$ cell–treated and saline-treated) were well separated on the panel, showing an obvious positive effect of CD34$^+$ cell injection on the blood flow in the peri-infarct zone after acute myocardial infarction. In fact, the average myocardial blood flow in the peri-infarct region in the absolute value was 0.988 ml/g per minute and 0.383 ml/g per minute for the cell-treated and saline-treated groups, respectively. Of note, the blood flow in the peri-infarct zone was ameliorated even in the animal with a ventricular aneurysm. On the other hand, the relative blood flow in the infarct to nonischemic region did not show

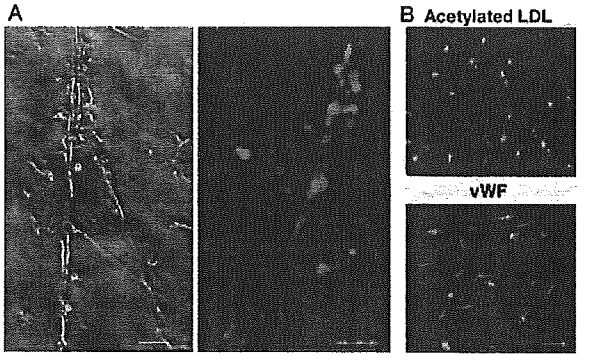

Figure 1. In vitro endothelial differentiation of cynomolgus CD34$^+$ cells lentivirally transduced with GFP. The transduced CD34$^+$ cells were differentiated to endothelial cells after 7 days in culture. **(A)**: Representative vessel-like structure derived from CD34$^+$ cells observed under a phase-contrast microscope (left) and a fluorescent microscope (right). **(B)**: The transduced CD34$^+$ cells differentiated into fluorescent cells (green) positive for the cellular intake of acetylated LDL and immunostaining for von Willebrand factor (vWF) (stained in red). Bar = 100 μm. Abbreviations: GFP, green fluorescent protein; LDL, low-density lipoprotein.

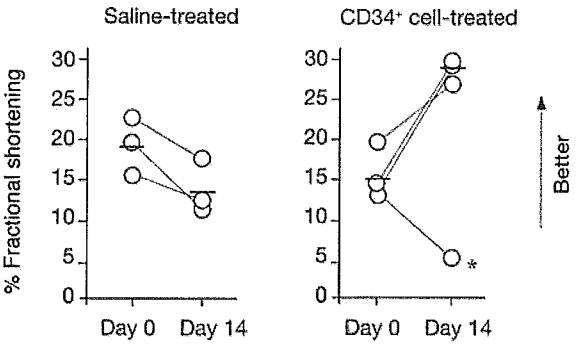

Figure 2. Improved cardiac function after CD34$^+$ cell transplantation. Cardiac function was assessed by echocardiography in terms of percent fractional shortening (%FS) before and 2 weeks after treatment. One monkey in the saline-treated group (CTR01061) died of heart failure 5 days after myocardial infarction and is not included in the figure. One monkey in the CD34$^+$ cell–treated group (*, BM01051) developed a left ventricular aneurysm after myocardial infarction. If this animal was excluded from the statistical analysis, the cardiac function was significantly improved in the CD34$^+$ cell–treated compared with the saline-treated group in terms of the ratio of %FS at day 14 versus day 0 after transplant ($p = .017$).

a significant difference between the CD34⁺ cell–treated and saline-treated groups. The peri-infarct region was the injection site, and thus the highest degree of change would be expected there.

All monkeys except one CD34⁺ cell–treated monkey (BM97080) were examined for cardiac function and blood flow at 2 weeks after transplantation, and their tissue sections were finally prepared at this time point (see below). BM97080 was examined at 12 weeks, at which time the cardiac function was still improved compared with immediately after infarction (data not shown) and the blood flow data were in a position similar to the cell-treated group at 2 weeks (Fig. 3C).

In Vivo Tracking of Transplanted Cells

Two weeks after the transplantation, tissue sections were prepared from the infarct, peri-infarct, and nonischemic regions. Immunostaining of an endothelial marker CD31 demonstrated more vessels in the peri-infarct region of the CD34⁺ cell-treated than saline-treated myocardium (Fig. 4A). In fact, the capillary density of the peri-infarct region was significantly better preserved in the cell-treated than saline-treated group, although there was no significant difference in the capillary density of the nonischemic control regions between the two groups (Fig. 4B).

Double immunostaining with anti-CD31 and anti-GFP showed that some cells in vessels were positive for both CD31 and GFP in the peri-infarct region (Fig. 5A). The result clearly indicates that at least some transplanted CD34⁺ cells gave rise to endothelial cells. However, we found that the transplanted cell progeny accounted for only a small fraction of endothelial cells after examining more than 100 sections of the peri-infarct region. In situ PCR for proviral GFP sequences also showed that few CD31-positive endothelial cells contained the GFP-provirus (Fig. 5B). There were no GFP-positive cardiomyocytes in more than 100 sections. Most of the transplanted cell progeny were found not incorporated in vessels (Fig. 5C). Hematoxylin-eosin staining did not show any noncardiac tissue regeneration in the myocardium.

On the other hand, we found that in vitro conditioned medium of CD34⁺ cell culture for endothelial differentiation contained high levels of VEGF, whereas unconditioned medium did not contain detectable VEGF, as assessed

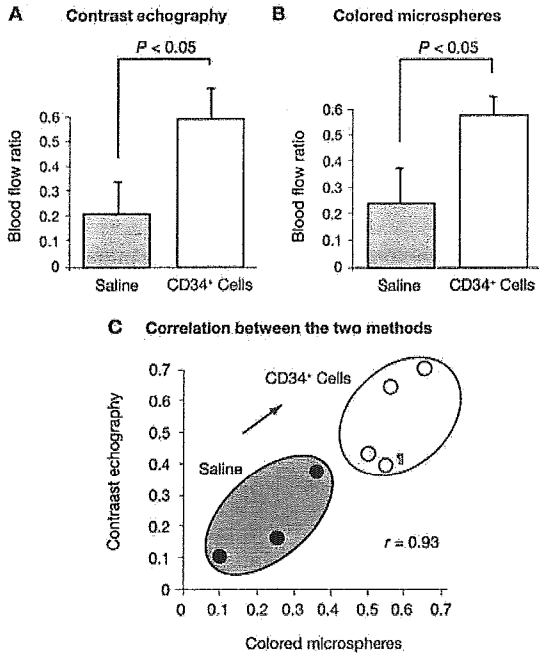

Figure 3. Improved regional blood flow after CD34⁺ cell transplantation. Myocardial contrast echocardiography **(A)** and colored microspheres **(B)** showed a significantly ameliorated blood flow ratio (the peri-infarct to nonischemic control region) in the CD34⁺ cell–treated monkeys ($n = 3$) compared with the saline-treated monkeys ($n = 3$) at 2 weeks after treatment. **(C)**: An excellent correlation was found between the two methods. A CD34⁺ cell–treated monkey (¶, BM97080) that was examined at 12 weeks after transplant is included in the panel **(C)** but excluded from the statistical analysis in **(A)** and **(B)**.

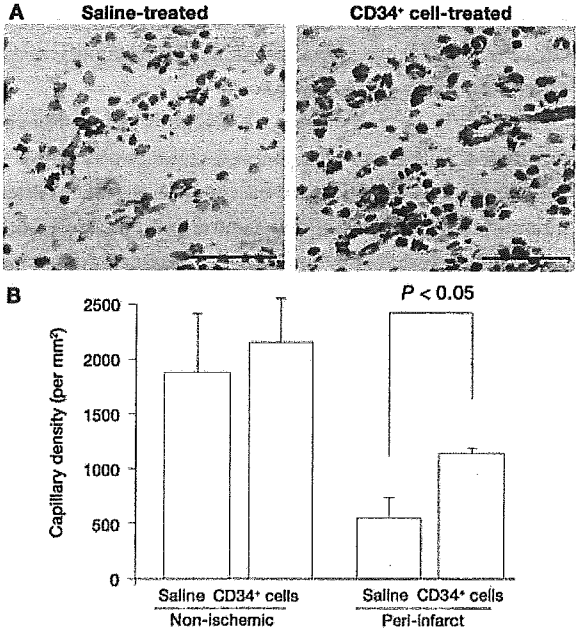

Figure 4. Neoangiogenesis in the ischemic myocardium. Tissue sections were prepared at 2 weeks after the treatment. **(A)**: Representative results of immunostaining with anti-CD31 (stained in brown) in the peri-infarct region of the saline-treated and CD34⁺ cell–treated myocardium. Bar = 50 μm. **(B)**: The density of CD31-positive capillaries in the peri-infarct and control nonischemic regions in the saline-treated and CD34⁺ cell–treated groups. Five fields for each section were randomly selected ($n = 3$ for the saline injection, $n = 3$ for the CD34⁺ cell injection), and the number of CD31-positive capillaries was counted (average ± standard deviation).